

Dual Antitumor and Antiangiogenic Activity of Organoplatinum(II) Complexes

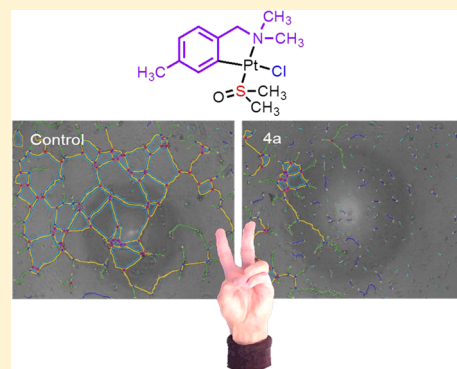
Ana Zamora,[†] Sergio A. Pérez,[†] Venancio Rodríguez,[†] Christoph Janiak,[‡] Gorakh S. Yello,[†] and José Ruiz*,[†]

[†]Departamento de Química Inorgánica and Regional Campus of International Excellence “Campus Mare Nostrum”, Universidad de Murcia, and Institute for Bio-Health Research of Murcia (IMIB-Arrixaca), E-30071 Murcia, Spain

[‡]Institut für Anorganische Chemie und Strukturchemie, Heinrich-Heine-Universität Düsseldorf, Universitätsstrasse 1, D-40225 Düsseldorf, Germany

Supporting Information

ABSTRACT: A library of over 20 cycloplatinated compounds of the type $[\text{Pt}(\text{dmbo-R})\text{LCl}]$ ($\text{dmbo-R} = \text{C}_2\text{N-dimethylbenzylamine-like ligand}$; R being MeO, Me, H, Br, F, CF_3 , and NO_2 substituents in the R_5 or R_4 position of the phenyl ring; L = DMSO and $\text{P}(\text{C}_6\text{H}_4\text{CF}_3\text{-p})_3$) has been prepared. All compounds are active in both human ovarian carcinoma A2780 cells and cisplatin-resistant A2780cisR cells, with most of the DMSO platinum complexes exhibiting IC_{50} values in the submicromolar range in the A2780 cell line. Interestingly, DMSO platinum complexes show low cytotoxicity in the nontumorigenic kidney cell line BGM and therefore high selectivity factors SF. In addition, some of the DMSO platinum complexes effectively inhibit angiogenesis in the human umbilical vein endothelial cell line EA.hy926. These are the first platinum(II) complexes reported to inhibit angiogenesis at a close concentration to their IC_{50} in A2780 cells, turning them into dual cytotoxic and antiangiogenic compounds.



INTRODUCTION

Ovarian epithelial carcinoma represents the fifth cause of cancer death in women, more than any other cancer of the female reproductive system.¹ Platinum drugs (Figure 1a) have dominated the therapy of ovarian and other gynecologic malignancies during the last three decades, and still now oxaliplatin and carboplatin are used in the different adjuvant treatments.² However, more than 90% of patients relapse with a chemoresistance problem, the major limitation of the current therapeutic concept, which has motivated a great interest to improve patient outcomes. From intraperitoneal chemotherapy to a targeted therapy, which promise personalized treatment, the most successful strategies are employing angiogenesis inhibitors.³ In 1970, Folkman proposed that tumor development and metastasis are angiogenesis-dependent, and hence, blocking angiogenesis could impede tumor growth. However, the limited survival benefits of antiangiogenic drugs stimulated interest in the combination of antiangiogenic drugs with established chemotherapies.^{4,5}

Cisplatin (CDDP) and its analogs tend to induce similar biological effects, whereas structurally different platinum compounds may lead to a different or complementary biological activity than that of the classical cross-linked DNA.⁶ Thus, coordination compounds have given way to organometallic compounds as leaders in the inorganic medicinal chemistry field.^{7–12} The stability of the transition metal complexes improves against reduction and ligand exchange reactions in the presence of a strong M–C σ bond.

Nowadays, cyclometalated C–N and C–N–N Pt^{II} complexes have been specifically designed with the ability to bind noncovalently to duplex DNA,¹³ targeting the human telomeric G-quadruplex^{13–15} or key proteins.^{13,16}

On the other hand, since the ruthenium compound NAMI-A demonstrated antimetastatic activity *in vivo*,¹⁷ more nontoxic ruthenium(II),^{18,19} rhodium(III),²⁰ and iridium(III)^{21,22} complexes have been published as angiogenesis inhibitors (Figure 1b). Furthermore, some bioactive metal compounds have a dual cytotoxicity and antiangiogenic properties,^{23–26} however, no platinum compounds have been published yet with a similar effect. Therefore, the synthesis and development of nonconventional new platinum compounds with dual activity could contribute to reduce the acquired-drug resistance and systematic toxicities generated by using either a cytotoxic or an antiangiogenic agent alone.

Based on promising results (Figure 1c),^{28–31} a systematic study of organometallic C,N-chelated antitumor platinum(II) complexes of the type $[\text{Pt}(\text{R-dmbo})\text{LCl}]$ has been developed. Dimethyl sulfoxide (DMSO) and tris(4-(trifluoromethyl)-phenyl)phosphine [$\text{P}(\text{C}_6\text{H}_4\text{CF}_3\text{-p})_3$] were used as ancillary ligands. We have also tried to elucidate any differences in their mode of action by the study of cell cycle arrest, apoptosis, and accumulation in both wild A2780 and its cisplatin-resistant variant A2780cisR. Furthermore, the intracellular localization

Received: October 20, 2014

Published: January 12, 2015

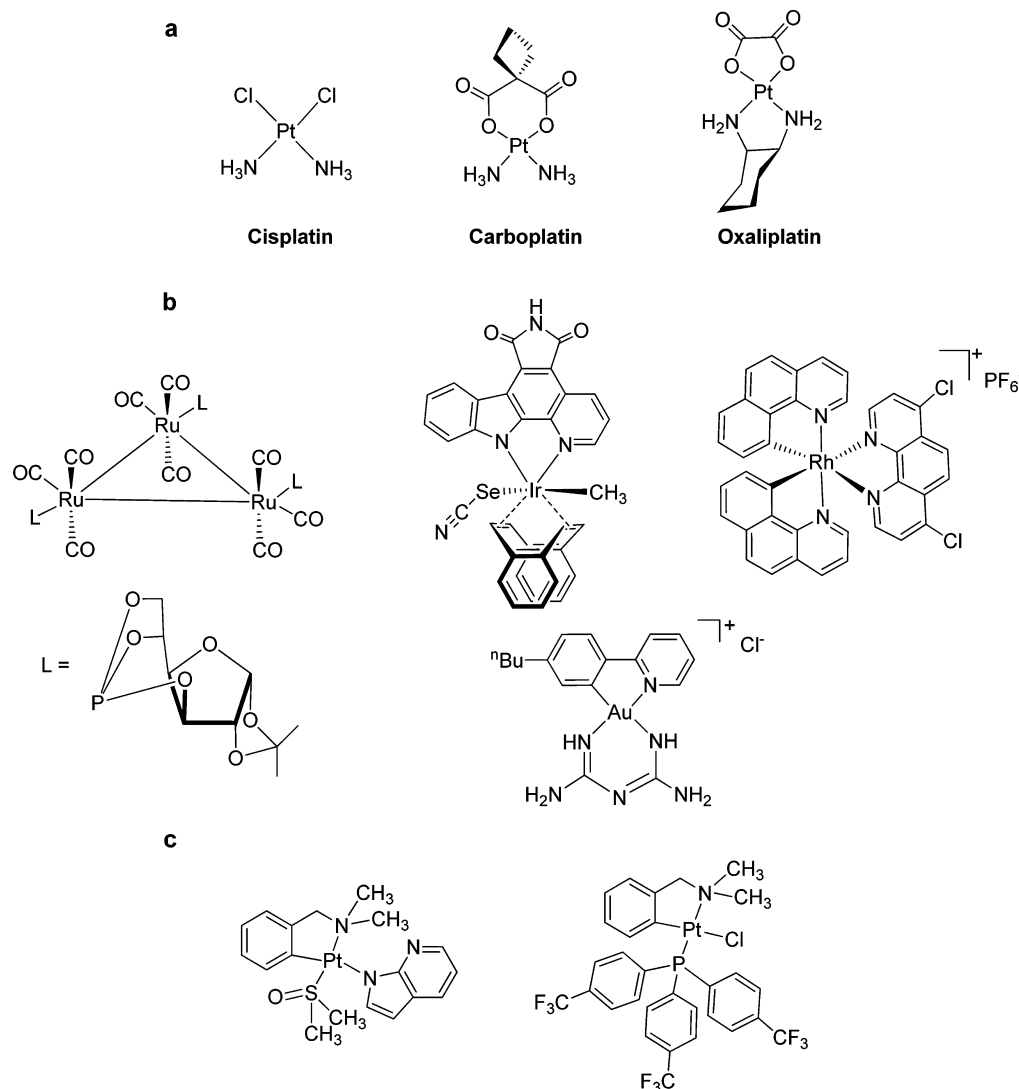
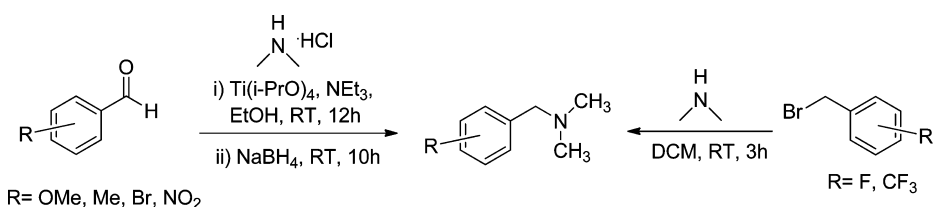


Figure 1. (a) Worldwide approved platinum drugs. (b) Some recent antiangiogenic metal complexes. (c) Some platinum complexes previously prepared by our group. The rhodium complex is an inhibitor of lipopolysaccharides (LPS)-induced NO production in RAW264.7 macrophages.²⁰ The staurospine-based iridium complex inhibits the protein kinase VEGFR3.²⁷ The ruthenium cluster and the gold complex have a dual cytotoxic and antiangiogenic activity.^{24,26} The 7-azaindolate platinum(II) complex showed potent anticancer activity against ovarian cancer.^{28,29} The fluorophosphine platinum(II) complex resulted to be more active than its triphenylphosphine analog and presented low RF values.³⁰

Scheme 1. Amine Formation



and morphological changes induced by selected new compounds have been studied by transmission electronic microscopy (TEM). The antiangiogenic activity of the DMSO complexes and migration of EA.hy926 cells (by wound healing assay) have also been studied. Throughout the analysis of a bioisosteres family, we have found suitable candidates for a subsequent biofunctionalization or encapsulation.

RESULTS AND DISCUSSION

Synthesis of Amines. Functionalized N,N-dimethylbenzylamines were prepared (Scheme 1) by reductive alkylations of dimethylamine,^{32,33} except for the fluoroamines, which were synthesized by nucleophilic substitution of the adequate benzyl bromide.³⁴

Synthesis and Characterization of Platinum Complexes. The cytotoxicity and pharmacokinetics of the complexes can be fine-tuned by ligand structures modifications, which has encouraged us to optimize the complex [Pt(R-

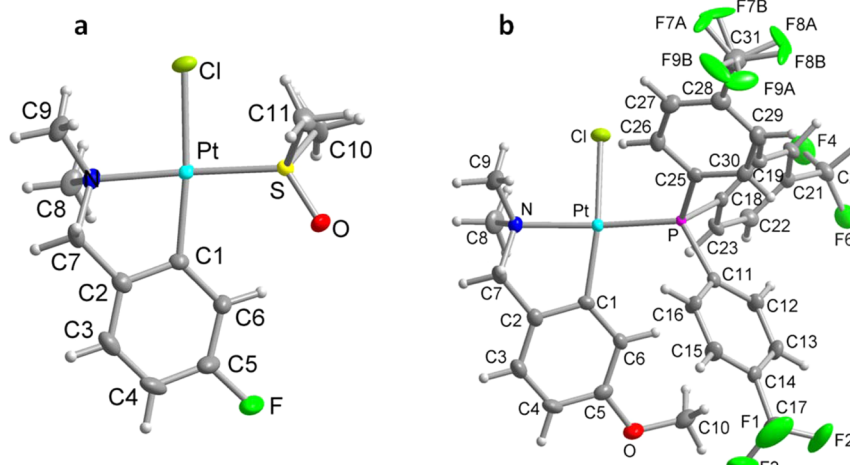
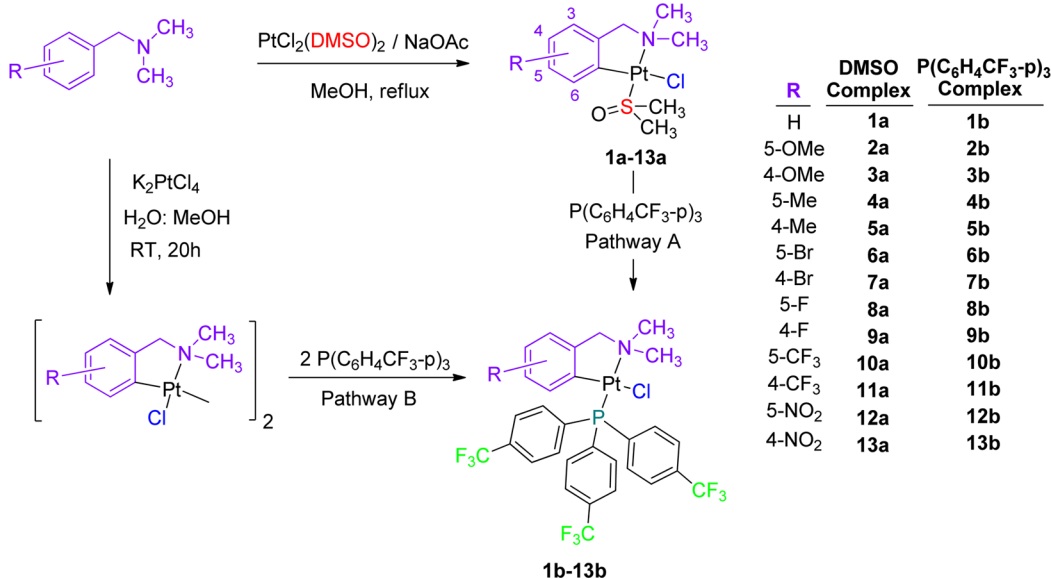
Scheme 2. Platinum Complexes Synthesis: Cyclometalation of R-dmba and Exchange of DMSO for P(C₆H₄CF₃-p)₃

Figure 2. Molecular structures with atom numbering schemes for (a) 8a (70% thermal ellipsoids) and (b) 2b (70% thermal ellipsoids, except for the disordered F atoms with 30% ellipsoids). One of the trifluoromethyl groups (C7–C9) is rotationally disordered. The disorder was refined for two approximately equally occupied positions (A and B) with the two (C)F₃ positions rotated by about 30° with respect to each other. Selected bond lengths (Å) and angles (deg) for 8a: Pt–C1 = 2.001(3), Pt–N = 2.113(2), Pt–S = 2.2112(7), Pt–Cl = 2.4006(7), C1–Pt–N = 81.03(11), N–Pt–Cl = 93.21(7), S–Pt–Cl = 89.02(2), C1–Pt–S = 97.00(8), N–Pt–S = 175.46(7), C1–Pt–Cl = 173.02(8). Selected bond lengths (Å) and angles (deg) for 2b: Pt–C1 = 2.004(2), Pt–N = 2.134(2), Pt–P = 2.2108(6), Pt–Cl = 2.3988(6), C1–Pt–N = 81.95(9), N–Pt–Cl = 91.54(6), P–Pt–Cl = 88.37(2), C1–Pt–P = 101.28(7), N–Pt–P = 162.97(6), C1–Pt–Cl = 162.97(7).

dmba)LCl] (dmba = *N,N*-dimethylbenzylamine, R = MeO, Me, H, Br, F, CF₃, and NO₂). Thus, we have investigated both the influence of introducing substituents (R) into the phenyl ring of the C–N ligand and the nature of the ancillary L-*trans*-to-NMe₂ ligand (L = DMSO or P(C₆H₄CF₃-p)₃) (Scheme 2).

DMSO platinum complexes 1a–13a were synthesized by cyclometalation of the PtCl₂(DMSO)₂ with the corresponding substituted *N,N*-dimethylbenzylamine. Cyclometalation was strongly influenced by the electronic effect of the R substituent; whereas donor groups such as MeO or Me promoted it, electro-withdrawing groups (especially NO₂) hindered it. This fact agrees with the idea that cyclometalation proceeds through an electrophilic C_{aryl}–H bond activation process.³⁵ On the other hand, phosphine derivatives 1b–13b were prepared easily by exchanging DMSO of 1a–13a for P(C₆H₄CF₃-p)₃ in CH₂Cl₂. They can also be prepared by a dimer compound

cleavage reaction with 2 equiv of the phosphine (Scheme 1, pathway B).

All the aforementioned derivatives were characterized by ¹H, ¹³C, and ¹⁹⁵Pt NMR spectroscopy. Also ³¹P and ¹⁹F NMR were used for phosphine or fluorinated complexes. ¹H NMR of DMSO platinum complexes 1a–13a are easily characterized because the resonances assigned to the methyls, CH₂, and H⁶ of the substituted *N,N*-dimethylbenzylamine-like ligand as well as the methyls of DMSO are flanked by ¹⁹⁵Pt satellites. P(C₆H₄CF₃-p)₃ complex formation is undoubtedly confirmed by the absence of a DMSO signal and the appearance of the H_o and H_m of P(C₆H₄CF₃-p)₃ signal. Furthermore, a H⁶ resonance displacement to high field (more shielded) is observed from DMSO to the P(C₆H₄CF₃-p)₃ complex, suggesting P-(C₆H₄CF₃-p)₃ is trans to NMe₂ (Supporting Information, Figure S1). The phosphine-*trans*-to-NMe₂ ligand geometry for

Table 1. IC_{50} (μM) for Cisplatin and Compounds 1a–13b at 48 h^a

Complex	A2780	A2780cisR	R	Complex	A2780	A2780cisR
1a	0.98 ± 0.07	2.12 ± 0.14	H	1b	3.36 ± 0.07	4.54 ± 0.86
2a	1.36 ± 0.05	2.22 ± 0.42	5-OCH ₃	2b	3.51 ± 0.08	4.44 ± 0.53
3a	1.08 ± 0.01	1.65 ± 0.20	4-OCH ₃	3b	4.01 ± 0.04	4.56 ± 0.22
4a	0.63 ± 0.18	1.97 ± 0.44	5-CH ₃	4b	4.67 ± 0.07	6.71 ± 0.61
5a	0.69 ± 0.01	1.54 ± 0.15	4-CH ₃	5b	4.89 ± 0.10	6.76 ± 0.13
6a	0.81 ± 0.08	1.48 ± 0.05	5-Br	6b	4.72 ± 0.06	7.40 ± 1.07
7a	0.96 ± 0.04	1.99 ± 0.45	4-Br	7b	5.99 ± 0.43	7.90 ± 0.32
8a	0.75 ± 0.19	2.24 ± 0.43	5-F	8b	4.52 ± 0.14	6.35 ± 0.57
9a	0.73 ± 0.10	1.49 ± 0.09	4-F	9b	4.17 ± 0.08	6.03 ± 0.87
10a	0.87 ± 0.14	1.13 ± 0.17	5-CF ₃	10b	4.06 ± 0.09	6.86 ± 0.08
11a	1.17 ± 0.20	2.40 ± 0.66	4-CF ₃	11b	9.96 ± 0.25	9.27 ± 2.19
12a	0.78 ± 0.05	2.29 ± 0.75	5-NO ₂	12b	6.16 ± 0.12	7.18 ± 0.62
13a	1.25 ± 0.34	3.65 ± 0.34	4-NO ₂	13b	5.58 ± 0.08	8.88 ± 0.57
CDDP	1.90 ± 0.20	19.57 ± 1.82				

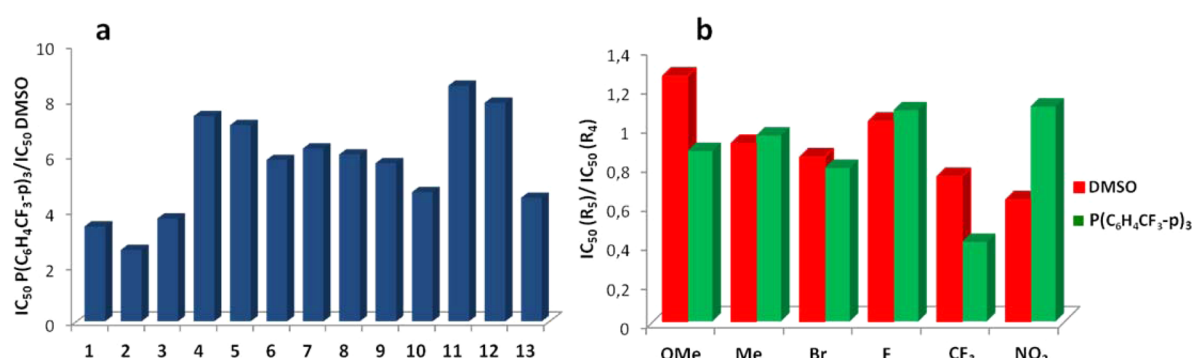
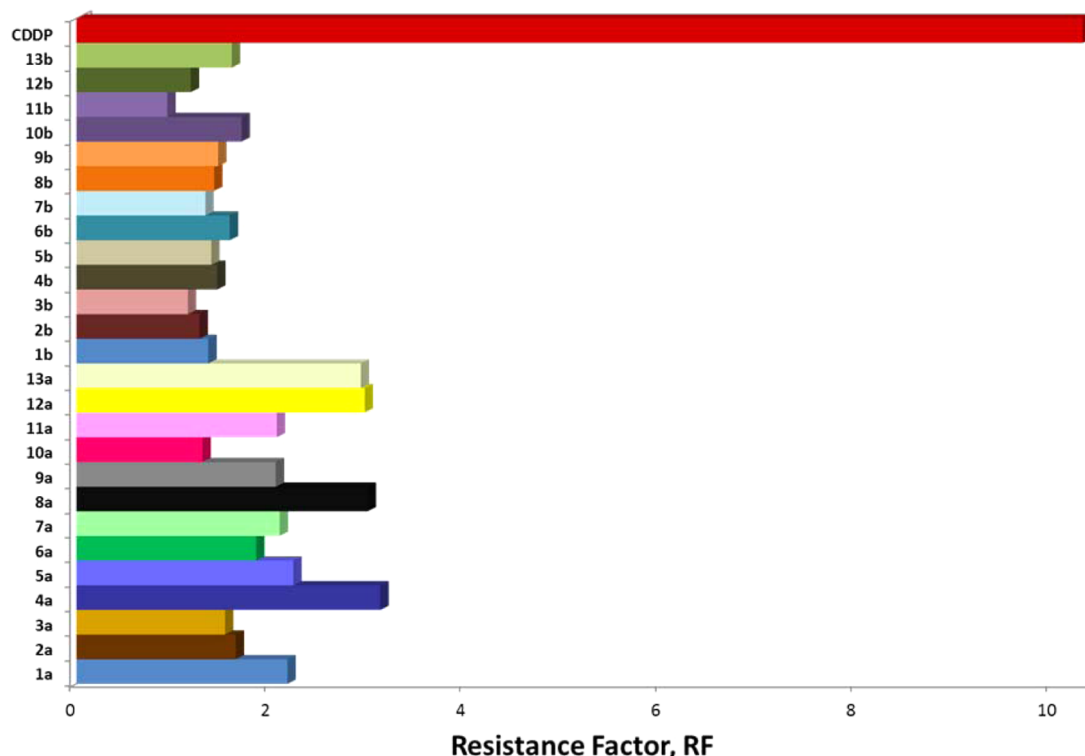
^aA2780: human ovarian cancer; A2780cisR: human resistant ovarian cancer.Figure 3. (a) Comparison of the ancillary ligand effect. The graph shows the ratio between phosphine and DMSO IC_{50} . (b) R substituent position effect. The graph shows the ratio between R_5/R_4 , red for DMSO complexes and green for $P(C_6H_4CF_3-p)_3$ analogs.

Figure 4. Resistance factors, RF, for CDDP and all the complexes studied toward CDDP-resistant A2780 human ovarian cancer cells, A2780cisR.

the **1b–13b** complexes was confirmed by the NOE effect between H_o of P(C₆H₄CF₃-p)₃ and H⁶ of the C–N chelating ligand and the X-ray of complex **2b** (Supporting Information, Figure S2). The positive-ion ESI-MS displayed the [M – Cl]⁺ peaks with the expected isotopic distribution pattern. All compounds were shown to be at least 95% pure by elemental analyses.

Structure Determinations. Single crystals suitable for X-ray diffraction analysis were obtained from the slow diffusion of hexane into a saturated solution of **8a** and **2b** in CH₂Cl₂/toluene. Their structures and atom numbering schemes are shown in Figure 2. Crystallographic data are shown in Tables S1 and S5 in the Supporting Information, and selected bond lengths and angles are listed in Tables S3 and S7 in the Supporting Information. For both compounds **8a** and **2b**, the Pt atom is in a distorted square planar environment, with the C–Pt–N bite angle deviating from 90° due to the bite of the cyclometalated ligand.^{29,30} As was suggested from NMR solution studies, the P(C₆H₄CF₃-p)₃ ligand in **2b** is positioned *trans* to the NMe₂ group, which automatically positions the chlorido ligand *trans* to the aryl ring of the C,N-chelate. The values of the Pt–C and Pt–N bond distances of the bonded dmiba ligand are within the normal ranges expected for such cyclometalated complexes.³⁶ The Pt–Cl bond distances in **8a** and **2b** are in the usual range.³⁷ The packing in the structure of **8a** is organized by intermolecular C–H···F,^{29,38,39} C–H···Cl,^{40,41} C–H···O,⁴² and C–H···π interactions^{43–48} (Supporting Information, Table S4 and Figure S3). There are no π–π interactions.^{49,50} The packing in the structure of **2b** is organized by fluorous (fluorine–fluorine) interactions. Parallel to the *bc* plane, the trifluoromethyl groups from different molecules are oriented toward each other to give a corrugated plane arrangement of these fluorous interactions (Supporting Information, Figures S4). Furthermore, packing in the structure of **2b** is also organized by intermolecular C–H···F,^{29,38,39} C–H···Cl,^{40,41} and C–F···π interactions (Supporting Information, Table S8 and Figures S5). There are no C–H···π^{43–48} or π–π interactions.^{49,50}

Biological Activity: Cytotoxicity Studies. The cytotoxicity of Pt^{II} complexes **1a–13a** and **1b–13b** was evaluated (Table 1 and Figures 3 and 4) toward human ovarian A2780 cancer cells and A2780cisR (acquired resistance to CDDP). Due to the low aqueous solubility of the complexes, the tested compounds were dissolved in DMSO first and then serially diluted in complete culture medium such that the effective DMSO content did not exceed 0.4%. CDDP, diluted in water, was used as positive control.

We investigated the effect on the cytotoxicity of MeO, Me, H, Br, F, CF₃, and NO₂ substituents in the R₅ and R₄ positions of the phenyl ring of the *N,N*-dimethylbenzylamine chelating ligand of the platinum complexes (Scheme 1). Their potency varied between 0.63 μM and 6.16 μM in the A2780 cell line, while the activity in A2780cisR ranged from 1.13 μM to 9.27 μM (Table 1). The following trends were observed:

- (a) DMSO complexes are more active than their phosphine counterparts and cisplatin. The ratio between the IC₅₀ values is higher than 3 in all the cases (Figure 3a).
- (b) There is not a clear structure–activity relationship after the introduction of the R substituent in DMSO complexes. These substituents do not modify drastically the anticancer activity of the parent compound, **1a**, so

that one may take advantage of the purpose of a later biofunctionalization.

- (c) The introduction of the R substituent in the P(C₆H₄CF₃-p)₃ complexes causes a reduction in the activity of **1b**.
- (d) Comparing the (R₅ vs R₄) isomeric couples **2/3**, **4/5**, **6/7**, **8/9**, **10/11**, and **12/13**, there was a slight preference for R₅-analogs. Only in the case of **2/3** for DMSO, and **8/9** and **12/13** for P(C₆H₄CF₃-p)₃ complexes, is the R₄-position (**3a**, **9b**, and **13b** complexes, respectively) preferred (Figure 3b).

Dmba Platinum Complexes Overcome the Acquired Resistance to CDDP.

On the other hand, A2780cisR encompasses all of the known major mechanisms of resistance to cisplatin:⁵¹ limitation of drug levels, enhanced DNA repair and/or increased damage tolerance, elevated cellular thiol (GSH) level, and failure of cell-death pathways. The compound's ability to overcome the acquired resistance was determined from the resistance factor, RF, defined as the ratio of resistant and sensitive IC₅₀. An RF of <2 is considered as the limit beyond which the compound denotes non-cross-resistance.⁵² In general, all the compounds are able to overcome the cisplatin resistance, and although some DMSO complexes show RF above 2, they are much lower than the cisplatin one (Figure 4).

DMSO Complexes **1a–13a** Are More Cell-Selective

than CDDP. Differential selectivity of an anticancer drug toward cancer cells versus normal cells increases the likelihood of tumor-specific cytotoxicity, reducing side effects in patients. Hence, the *in vitro* antiproliferative activity of DMSO compounds and CDDP was also evaluated in a kidney healthy cell line, BGM (African green monkey kidney) (Table 2). All

Table 2. IC₅₀ (μM) for CDDP and Compounds **1a–13a** at 48 h

Complex	BGM	EA.hy926
1a	6.55 ± 0.20	6.32 ± 0.12
2a	11.27 ± 0.32	9.67 ± 0.13
3a	7.34 ± 0.32	6.88 ± 0.10
4a	10.87 ± 0.65	6.20 ± 0.11
5a	8.44 ± 0.32	5.72 ± 0.23
6a	7.44 ± 0.36	5.24 ± 0.09
7a	7.97 ± 0.30	4.97 ± 0.18
8a	6.46 ± 0.41	6.09 ± 0.11
9a	9.07 ± 1.71	6.30 ± 0.11
10a	6.31 ± 0.11	4.50 ± 0.08
11a	9.33 ± 1.31	7.55 ± 0.27
12a	9.61 ± 0.78	6.90 ± 0.14
13a	15.49 ± 2.55	10.51 ± 0.29
CDDP	4.25 ± 0.37	9.86 ± 0.64

the complexes were found to be less toxic than cisplatin in the kidney cell line. More importantly, selectivity factor values (SF = kidney normal cells IC₅₀ divided by the ovarian malignant cells IC₅₀) attest to a preferential cytotoxicity of Pt^{II} organometallic complexes toward neoplastic cells. The cell selectivity factors for **1a–13a** are higher (up to SF = 17.25 for **4a**) than that of CDDP (SF = 2.24) (Figure 5). That may contribute to overcome nephrotoxicity, which is one of the most aggressive side effects of chemotherapy.

On the other hand, IC₅₀ values for **1a–13a** in the EA.hy926 cell line were also calculated (Table 2) with the aim to verify

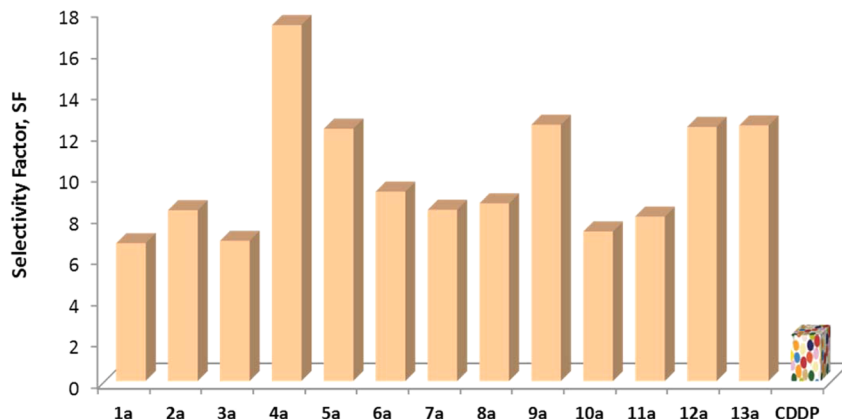


Figure 5. Selectivity factors, SF, of DMSO complexes and CDDP.

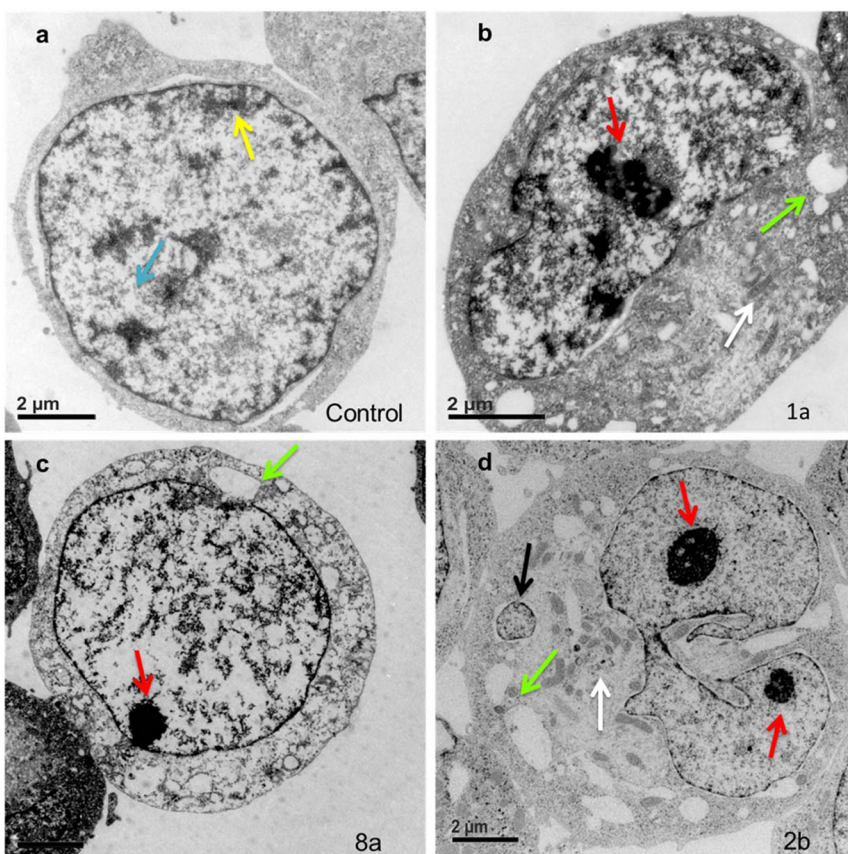


Figure 6. TEM images of (a) untreated A2780 cells, and A2780 cells after 24 h of exposure at 310 K to 1 μ M of (b) 1a, (c) 8a, and 4 μ M of (d) 2b. Yellow and blue arrows indicate heterochromatin and euchromatin in the control, respectively. Red arrows signalize nucleolus, green vacuoles, and white mitochondria in the cells treated with compounds. The black arrow in (d) shows part of the nucleus embedded in a vacuole.

that the antiangiogenic effect was not due to a cytotoxic effect but rather to their antiangiogenic potential.

Distribution of Platinum Using Transmission Electron Microscopy (TEM). By using TEM, it seemed likely that we would observe platinum derived contrast in sections of cancer cells treated with the platinum complexes studied here if their deposition is sufficiently localized in cell organelles. A2780 cells were exposed to 1 μ M of 1a (the parent compound), 8a (a very active DMSO derivative), and 2b (a very active phosphine compound) for 24 h at 310 K, and the treated and control cells were fixed and embedded in epoxy resin. Ultrathin sections were observed under the TEM (Figure 6). No uranyl acetate or

OsO_4 was used for staining both the control cells and the treated cells. Any additional contrast observed between the control cells and the treated cells is due to cell uptake of the platinum complexes. Sections of cells treated with 1a, 8a, and 2b show more contrast in comparison to those from control cells, in particular in the nucleolus, and the internal nuclear membrane (Figure 6b–d). The results suggest that these compounds interact with the nucleic acids of the nucleus. Several cells displayed the morphological changes associated with apoptosis,⁵³ such as intact cell membrane even late in the cell disintegration phase, nuclear fragmentation (Figure 6d), disorganized cytoplasmic organelles (white arrow), and large

clear vacuoles (green arrows). During the chromatin condensation at an early apoptosis phase, the electron-dense nuclear material characteristically aggregates peripherally under the internal nuclear membrane (Figure 6c), whereas cells fragment into apoptotic bodies with intact cell membranes in the later phase of apoptosis (Figure 6d).

Accumulation Studies. Acquired resistance is known as the major disadvantage to CDDP treatment. Among the several explanations that can account for CDDP resistance, decreased cellular accumulation of the drug appears to be one important mechanism. The cellular accumulation of the Pt^{II} complexes in the A2780 and A2780cisR ovarian cancer cell lines was studied to investigate the possible relationship between cellular uptake, cytotoxicity, and resistance. Cellular concentrations were determined by ICP-MS after 24 h of exposure to the most active compound **4a**, its phosphine analog **4b**, and CDDP at 1, 4, and 2 μ M, respectively. The results are summarized in Figure 7. As a general result, the cellular accumulation of the

complexes increases in the sensitive A2780 with respect to the resistant A2780cisR. Indeed, complex **4a** accumulates more effectively than **4b** and CDDP, which correlates with their IC₅₀ values. It is also interesting to note that the ratio of the Pt levels of A2780cisR/A2780 increases following the trend **4b** > **4a** > CDDP, resulting in the higher RF values for CDDP > **4a** > **4b**.

Cell Cycle Arrest. To understand the effect of Pt^{II} derivatives on cell growth, we examined the effect of some DMSO and two phosphine derivatives on the cell cycle by FACS (fluorescence activated cell sorter) analysis. After treatment of A2780 cell lines with 1 μ M of **1a**, **2a**, **4a**, **8a**, and CDDP or 4 μ M of **1b** and **2b** (approximately the IC₅₀ value for the platinum derivatives with respect to A2780 cells) for 24 h (Figure 8 and Supporting Information, Figure S6), we found two different behaviors. Whereas compounds **2a**, **4a**, **1b**, and **2b** arrest the cycle in the G0/G1 phase, **1a** and **8a** lead to the appearance of a nondividing tetraploid and arrest the cycle in the S/G2 phase. Both cases diverge from the large disruption caused by CDDP, which arrests the cycle in the S phase, as the population increment with respect to the control shows.

On the other hand, Figure S7 in the Supporting Information shows cell cycle arrest for the same compounds in A2780cisR. The new organometallic complex causes a slight increment in the population of the G0/G1 (phosphine derivatives) and S/G2 (DMSO derivatives) phases, again in contrast with that generated by CDDP in the S phase.

Apoptosis Studies. Apoptotic studies were also carried out with the A2780 cell line. Exposure of phosphatidylserine (PS) was followed by a flow cytometric assay with the Annexin V-FLUOS apoptosis detection kit (Roche). Propidium iodide (PI) was also applied to stain necrotic or late apoptotic cells. Fluorescence intensity was measured for each cell by flux cytometry. The results are shown in Figure 9 and Figure S8 in the Supporting Information. The four typical quadrants

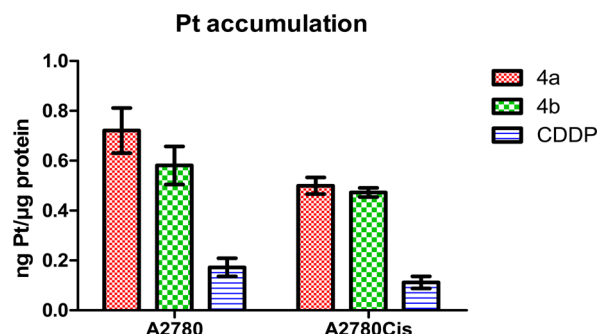


Figure 7. Intracellular platinum accumulation in A2780 and A2780cisR cells at 24 h incubation with complexes **4a**, **4b**, and CDDP.

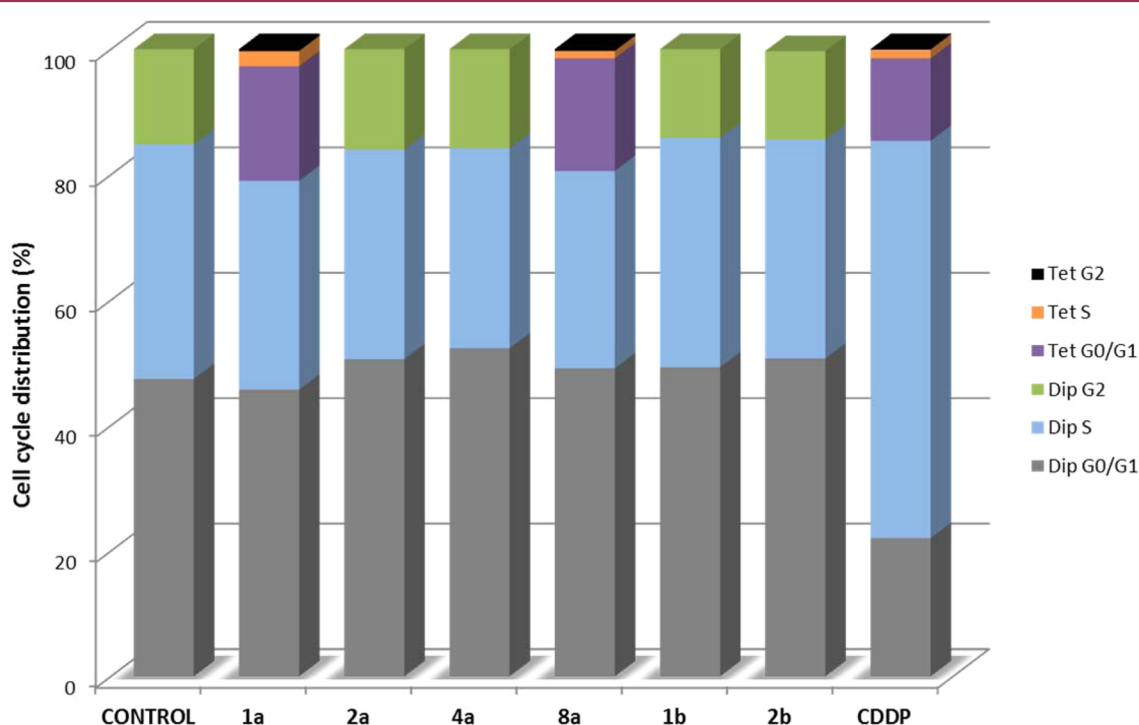


Figure 8. Cell cycle analysis of A2780 human ovarian cancer cells after 24 h treatment with approximately the IC₅₀ value for the platinum derivatives at 310 K.

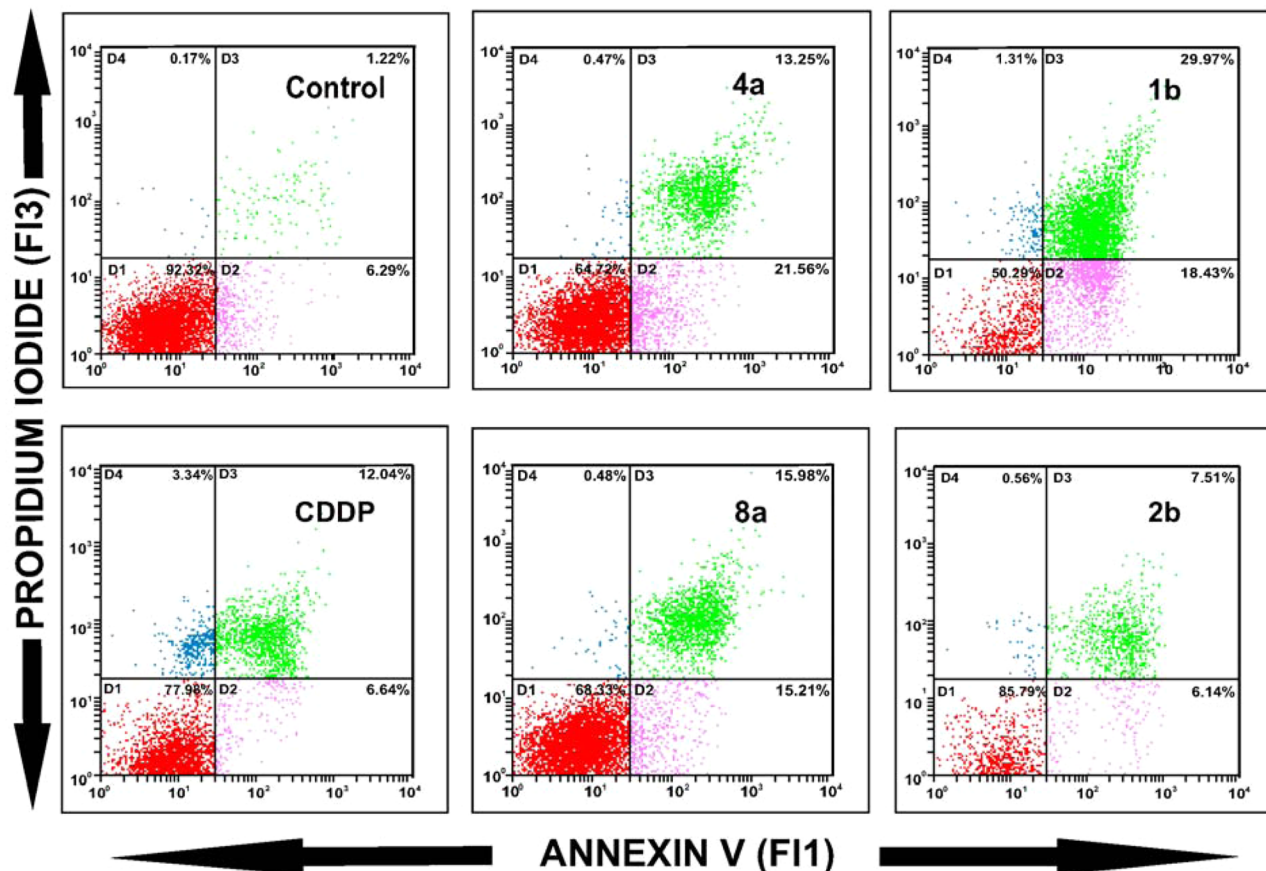


Figure 9. Flow cytometry analysis of A2780 human ovarian cancer cells after treatment with 4a, 8a, 1b, and 2b as detected by annexin V/PI. Density plots for untreated cells (control) and for cells treated with 2 μ M (24 h) of 4a, 8a, and CDDP and cells treated with 8 μ M (24 h) of 1b and 2b. The experiments were performed in triplicate.

identifying the living (lower left quadrant D1, not or low stained cells), the early apoptotic (lower right quadrant D2, only the annexin-V stained cells), the necrotic (upper left quadrant D4, only PI stained cells), and the late apoptotic (upper right quadrant D3, cells stained with both fluorescent dyes) cells appear in these diagrams. As can be seen clearly, 4a, 8a, and 1b induce a high incidence of apoptosis (35%, 31% and 48%, respectively) in A2780 cells at 24 h without increasing the necrotic population. The same study for 4a at 48 h showed an increase in annexin V-positive apoptotic cells (86%) (Supporting Information, Figure S9), demonstrating that complex 4a induced apoptosis in a time-dependent manner.

It seems that DNA damage, caused before the S phase (G1 checkpoint) and after (G2 checkpoint), could not be repaired, preventing the cell from arriving at the next phase, so that the cell would die by apoptosis. We have confirmed DNA damage is consistent with cell death, which occurs through the apoptosis process. The cell shrinkage and morphology shown in Figure 6 were also consistent with this type of cell death.

Apoptosis experiments in A2780cisR after 24 h of incubation with DMSO derivatives (Supporting Information, Figure S10) show a diminution of the percentage of apoptotic cells, in contrast with the increment caused by phosphine derivatives. Again, this is another sign of how phosphine derivatives overcome cisplatin-resistance.

Reactions of the Platinum Complexes with 9-Ethylguanine Followed by ^1H NMR. Once nucleic acids of nucleus were identified as the most likely primary biological

target of both the DMSO and $\text{P}(\text{C}_6\text{H}_4\text{CF}_3\text{-p})_3$ families of compounds, we wondered whether the interaction with DNA would take place by covalent binding to guanine. That is the reason why we carried out the reactions of the complexes 8a and 2b with the model nucleobase 9-EtG in a 1:5 ratio. Both reactions were followed by ^1H NMR in a $\text{D}_2\text{O}/\text{DMSO}-d_6$ (1:4) mixture at 310 K (Supporting Information, Figures S11 and S12), observing that, in the reaction with complex 2b, 9-EtG was completely bound to platinum in less than 30 min, whereas for 8a the reaction occurred only in 50%. In both cases monofunctional adducts were formed.

No Hoechst 33258 Displacement Took Place. In order to clarify the binding mode between the new metal complexes and DNA, a fluorescence competition experiment with Hoechst 33258 was employed. This ligand is able to bind via electrostatic interactions to the minor groove of duplex DNA (with marked preference for AT-rich regions) at high DNA/Hoechst ratio.⁵⁴ Due to the fluorescence yield of Hoechst 33258 increasing significantly in the presence of DNA, an intensity reduction with complexes addition is interpreted as the displacement of Hoechst bound to ct-DNA. None of the studied complexes was able to produce a decrease in the Hoechst bound to DNA spectra (Supporting Information, Figure S13), which means the complexes do not bind in the minor groove of DNA. This result is in agreement with the hypothesis that the Pt^{II} complexes are able to bind covalently to DNA.

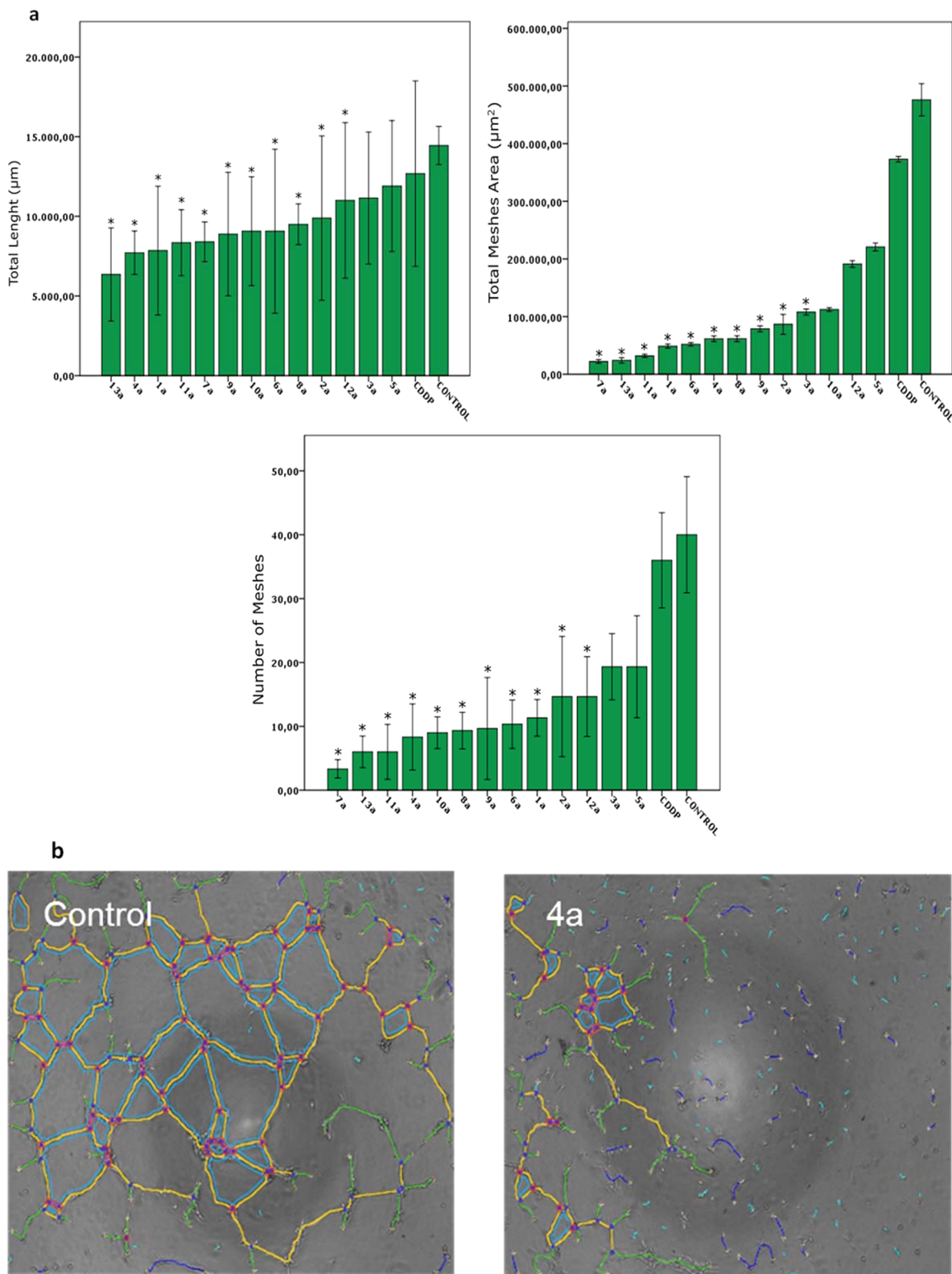


Figure 10. Effect of the DMSO complexes in the endothelial cell tube formation assay. (a) Quantification after the ImageJ process of number of meshes, total meshes area, and total length of the tubular structure of EA.hy926 cells under $1 \mu\text{M}$ of compounds **1a–13a** and CDDP for 12 h. Error bars represent the standard deviation of three independent experiments. * $p < 0.05$ was considered to be statistically significant. (b) Typical images after an ImageJ process of EA.hy926 cells added to 24-well plates precoated with Matrigel for 12 h: for culture medium as a control and with **4a**, $1 \mu\text{M}$. Tube formation of EA.hy926 cells was photographed under an inverted phase-contrast microscope.

Inhibition of Tube Formation by DMSO Complexes **1a–13a in EA.hy926 Endothelial Cells.** Angiogenesis is often assessed by the ability of endothelial cells to sprout,

migrate, and form vascular tubes *in vitro* on a Matrigel matrix, a gelatinous protein mixture secreted by Engelbreth-Holm-Swarm (EHS) mouse sarcoma cells.^{55,56}

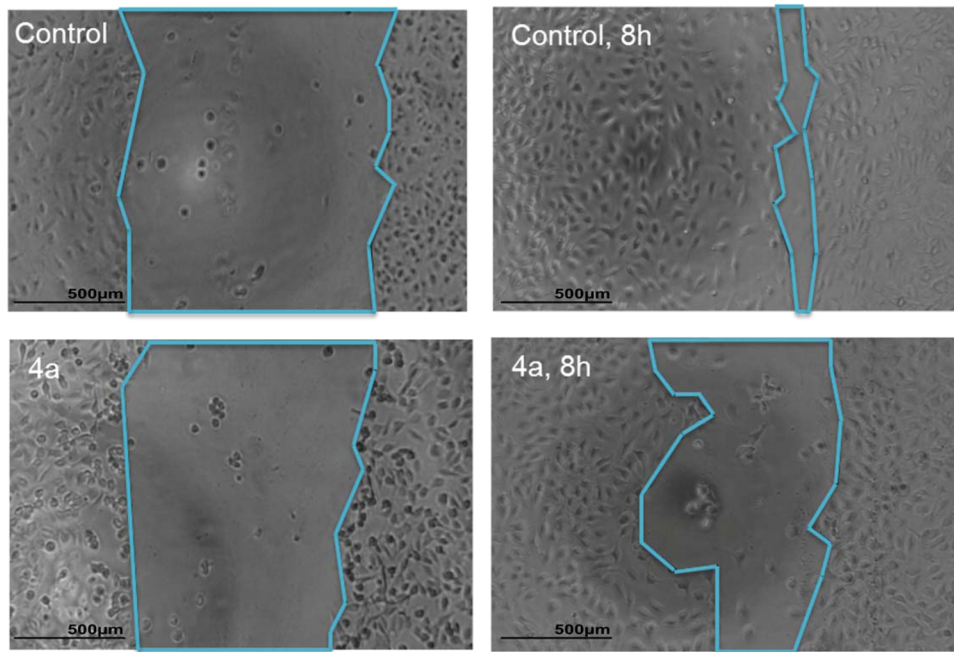


Figure 11. Effect of compound **4a** on the migration of EA.hy926 cells by wound healing assay. Typical images of the wound at the beginning of the experiment and after 8 h for culture medium as a control and with **4a**, 1 μ M. Migration of EA.hy926 cells was photographed under a light microscope (scale bar, 500 μ m), and the data were digitally recorded.

In vitro angiogenesis was measured 12 h after incubating EA.hy926 cells with DMSO compounds **1a–13a** at 5, 3, and 1 μ M concentrations (Figure 10b and Supporting Information, Figure S14). The concentration reduction was carried out in order to work at its subcytotoxic concentration (Table 2). The resulting formation or inhibition of capillary-like structures was quantified only for 1 μ M (Figure 10a) using a combination of the three most representative parameters: total length (μ m), number of meshes (network or polygonal structures), and total meshes area (area occupied by the meshes, μ m 2).

Only those compounds that presented significant differences in all the studied parameters were considered antiangiogenic. Thereby, apart from CDDP, there are only four compounds (**3a**, **5a**, **10a**, and **12a**) that do not display antiangiogenic activity at 1 μ M. The rest of them inhibit the formation of vascular tubes not only at subcytotoxic concentrations (3 μ M) but also at one very close to their IC₅₀ in A2780 cells. This fact turns them into dual cytotoxic and antiangiogenic compounds.

Effect of DMSO Complexes **1a–13a on the Migration of EA.hy926 Cells by Wound Healing Assay.** As a second indication of the activity of compounds **1a–13a** in endothelial cells function, we performed a migration study. It is based on the scratch of the cells and the measurement of their ability to close it after 8 h with or without the addition of the compounds.⁵⁷ Figure 11 shows clearly how compound **4a** diminished the mobility of EA.hy926 cells with respect to the control, which was almost fully repopulated.

Since EA.hy926 cells were not affected by the exposure to the compounds at 1 μ M in that short period of time, the inhibition of migration is likely to result from antiangiogenic activity.

Figure 12 summarizes the results for DMSO complexes **1a–13a** and CDDP as the percentage of cell-free area after 8 h. (Wound healing area (%) = [cell-free area (0 h) – cell-free area (8 h)]/cell-free area (0 h) \times 100).

Compounds **2a**, **3a**, **8a**, and **9a** did not inhibit the migration at the tested concentration. Thus, and taking into account both

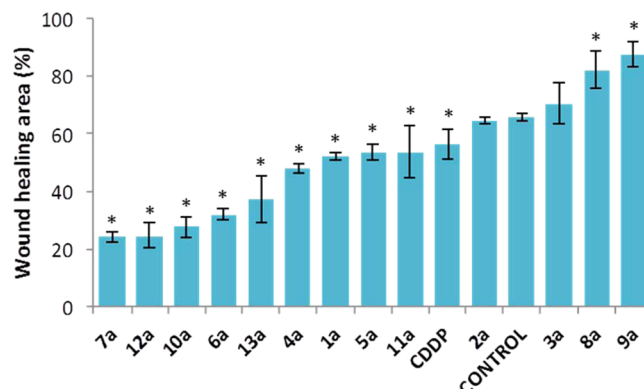


Figure 12. Effect of compounds **1a–13a** and CDDP on the migration of EA.hy926 cells by a wound healing assay. EA.hy926 cells were treated with 1 μ M of compounds **1a–13a** and CDDP for 8 h. * p < 0.05 was considered to be statistically significant.

experiments in endothelial cells, compounds **1a**, **4a**, **6a**, **7a**, **11a**, and **13a** display prominent antiangiogenic properties at a cytotoxic concentration in A2780 cells.

CONCLUSIONS

A small library of over 20 compounds of the type [Pt(N-C)LCl] (N-C = *C,N*-dimethylbenzylamine-like ligand; L = DMSO and P(C₆H₄CF₃-p)₃) have been prepared. All of them are active in the CDDP resistant cells A2780cisR and have shown strong apoptosis inducing character *in vitro*. The DMSO platinum complexes trigger strong cytotoxic effects (in submicromolar IC₅₀ values in A2780), being more active than their phosphine counterparts (low micromolar IC₅₀) and CDDP. The toxicity toward the nontumorigenic cells BGM of the new compounds is less than that of CDDP. The cell selectivity factors (SF = ratio of IC₅₀ for BGM/IC₅₀ for A2780 cells) for **1a–13a** are higher (up to SF = 17.25 for **4a**) than that

of CDDP ($S_F = 2.24$). Comparing the (R5 vs R4) isomeric couples **2/3**, **4/5**, **6/7**, **8/9**, **10/11**, and **12/13**, there was only in the case of **2/3** a clear preference for the R4-analogue **3a**. TEM images showed high electron density in both heterochromatin and nucleolus of A2780 cells incubated with selected compounds. In addition, some of the DMSO platinum complexes inhibited effectively angiogenesis in the human umbilical vein endothelial cell line EA.hy926 at $1 \mu\text{M}$. Tube formation from EA.hy926 has been quantified with ImageJ software, and the study of the effect of DMSO complexes on the migration of EA.hy926 cells by wound healing assay has also been undertaken. Complexes **1a**, **4a**, **6a**, **7a**, **11a**, and **13a** are the first platinum(II) complexes reported to inhibit angiogenesis at a concentration close to the A2780 IC₅₀. Therefore, these are potent agents with dual antiangiogenic and cytotoxic activities.

■ EXPERIMENTAL SECTION

General Methods and Starting Materials. The C, H, N and S analyses were performed with a Carlo Erba model EA 1108 microanalyzer. The ¹H, ¹³C, ³¹P, ¹⁹F, and ¹⁹⁵Pt NMR spectra were recorded on a Bruker AC 300E or a Bruker AV 400 spectrometer. Chemical shifts are cited relative to SiMe₄ (¹H and ¹³C, external), CFCl₃ (¹⁹F, external), 85% H₃PO₄ (³¹P, external), and Na₂[PtCl₆] (¹⁹⁵Pt, external). ESI mass (positive mode) analyses were performed on a HPLC/MS TOF 6220. The isotopic distribution of the heaviest set of peaks matched very closely that calculated for the formulation of the complex cation in every case. UV-vis spectroscopy was carried out on a PerkinElmer Lambda 750 S spectrometer with operating software. Fluorescence measurements were carried out with a PerkinElmer LS 55 50 Hz Fluorescence Spectrometer. PerkinElmer ScieX Elan 6000 DRC-e ICP-MS instrument (PerkinElmer, Norwalk, CT) was used to determine Pt concentration.

All synthetic manipulations were carried out under an atmosphere of dry, oxygen-free nitrogen using standard Schlenk techniques. Solvents were dried by the usual methods. *N,N*-dimethylbenzylamine, tris(4-(trifluoromethyl)phenyl)phosphine, substituted benzaldehydes, 3-fluorobenzyl bromide, 4-fluorobenzyl bromide, titanium(IV) isopropoxide, sodium borohydride, sodium salt of calf thymus DNA, ethidium bromide (EB), and Hoechst 33258 were obtained from Sigma-Aldrich (Madrid, Spain), dimethylamine from Fluka and K₂PtCl₄ from Johnson Matthey. Deuterated solvents were obtained from Euriso-top. Pt(DMSO)₂Cl₂ and [Pt(dmba)(μ -Cl)]₂ were prepared using reported procedures.^{58,59} Complexes **1a**, **1b**, **8b** and **10b** were synthesized using literature procedure.^{30,60} All synthesized platinum compounds were isolated in $\geq 95\%$ purity, as determined by elemental analyses.

General Procedure for the Synthesis of Cycloplatinated DMSO Pt(II) Complexes 1a–13a. The method was adapted from the previously described by van Koten.⁶⁰ The corresponding amine (0.71 mmol) dissolved in MeOH (2 mL) was added under N₂ to a suspension of PtCl₂DMSO₂ (0.71 mmol) and NaOAc (1.4 mmol) in 15 mL of freshly distilled MeOH. The resulting mixture was stirred at 65 °C and the reaction time that ranged from 4 to 24 h depending on the amine, was monitored by TLC. When the reaction finished, the solution was concentrated under vacuum and a white or yellow solid precipitated. The solid was filtrated, washed with MeOH/ether and air-dried.

Complex 2a. White solid. Yield: 51%. Anal. Calcd for **2a** C₁₂H₂₀ClNO₂PtS: C, 30.48; H, 4.26; N, 2.96; S, 6.78. Found: C, 29.85; H, 4.06; N, 2.82; S, 6.55. ¹H NMR (300 MHz, DMSO-*d*₆): δ 7.41 (d, 1H, H⁶, J_{H6H4} = 2.7 Hz, J_{Hpt} = 53.1 Hz), 6.95 (d, 1H, H³, J_{H3H4} = 8.1 Hz), 6.53 (dd, 1H, H⁴, J_{H4H3} = 8.1 Hz, J_{H4H6} = 2.7 Hz), 3.92 (s, 2H, CH₂N, J_{Hpt} = 40.5 Hz), 3.61 (s, 3H, OCH₃), 2.73 (s, 6H, N(CH₃)₂, J_{Hpt} = 30.3 Hz). ¹³C{¹H} NMR (75.46 MHz, DMSO-*d*₆): δ 121.91 (s, CH³), 119.60 (s, CH⁶), 109.17 (s, CH⁴), 73.04 (s, CH₂N), 54.69 (s, OCH₃), 51.47 (s, N(CH₃)₂). ¹⁹⁵Pt NMR (86.18 MHz,

DMSO-*d*₆): δ -3645.17 (s). ESI-MS (pos. ion mode, CH₂Cl₂): *m/z* 437.06 ([M - Cl]⁺, calcd. 437.08).

Complex 3a. White solid. Yield: 79%. Anal. Calcd for **3a** C₁₂H₂₀ClNO₂PtS: C, 30.48; H, 4.26; N, 2.96; S, 6.77. Found: C, 30.45; H, 4.20; N, 2.99; S, 6.78. ¹H NMR (300 MHz, CDCl₃): δ 7.82 (d, 1H, H⁶, J_{H6H5} = 8.4 Hz, J_{Hpt} = 46.2 Hz), 6.63 (m, 2H, H⁵+H³), 3.94 (s, 2H, CH₂N, J_{Hpt} = 39.9 Hz), 3.74 (s, 3H, OCH₃), 3.51 (s, 6H, SCH₃, J_{Hpt} = 24.9 Hz), 2.90 (s, 6H, N(CH₃)₂, J_{Hpt} = 33.3 Hz). ¹³C{¹H} NMR (150.9 MHz, CDCl₃): δ 134.97 (s, CH⁶, J_{CPt} = 89.2 Hz), 111.14 (s, CH⁵, J_{CPt} = 87.7 Hz), 108.62 (s, CH³, J_{CPt} = 55.7 Hz), 74.96 (s, CH₂N, J_{CPt} = 75.9 Hz), 55.43 (s, OCH₃), 52.47 (s, N(CH₃)₂), 46.98 (s, SCH₃, J_{CPt} = 94.6 Hz). ¹⁹⁵Pt NMR (86.18 MHz, CDCl₃): δ -36766.62 (s). ESI-MS (pos. ion mode, CH₂Cl₂): *m/z* 437.08 ([M - Cl]⁺, calcd. 437.08).

Complex 4a. White solid. Yield: 58%. Anal. Calcd for **4a** C₁₂H₂₀CINOPtS: C, 31.55; H, 4.41; N, 3.07; S, 7.02. Found: C, 31.55; H, 4.42; N, 3.10; S, 7.05. ¹H NMR (400 MHz, CDCl₃): δ 7.78 (s, 1H, H⁶, J_{Hpt} = 46.0 Hz), 6.96 (d, 1H, H³, J_{H3H4} = 7.2 Hz), 6.89 (d, 1H, H⁴, J_{H4H3} = 7.2 Hz), 3.96 (s, 2H, CH₂N, J_{Hpt} = 39.6 Hz), 3.54 (s, 6H, SCH₃, J_{Hpt} = 22.8 Hz), 2.91 (s, 6H, N(CH₃)₂, J_{Hpt} = 33.2 Hz), 2.32 (s, 3H, Me). ¹³C{¹H} NMR (150.9 MHz, CDCl₃): 134.86 (s, CH⁶, J_{CPt} = 79.2 Hz), 125.76 (s, CH⁴), 121.56 (s, CH³, J_{CPt} = 55.1 Hz), 74.84 (s, NCH₂, J_{CPt} = 78.9 Hz), 52.32 (s, N(CH₃)₂), 46.95 (s, SCH₃, J_{CPt} = 94.5 Hz), 21.88 (s, CH₃). ¹⁹⁵Pt NMR (86.18 MHz, CDCl₃): δ -3665.38 (s). ESI-MS (pos. ion mode, CH₂Cl₂): *m/z* 421.09 ([M - Cl]⁺, calcd. 421.09).

Complex 5a. White solid. Yield: 85%. Anal. Calcd for **5a** C₁₂H₂₀CINOPtS: C, 25.32; H, 3.28; N, 2.68; S, 6.15. Found: C, 25.31; H, 3.26; N, 2.69; S, 6.15. ¹H NMR (400 MHz, CDCl₃): δ 7.81 (d, 1H, H⁶, J_{H6H5} = 8.0 Hz, J_{Hpt} = 40.4 Hz), 6.89 (s, 1H, H³), 6.86 (d, 1H, H⁵, J_{H5H6} = 8.0 Hz), 3.95 (s, 2H, CH₂N, J_{Hpt} = 40.0 Hz), 3.53 (s, 6H, SCH₃, J_{Hpt} = 23.6 Hz), 2.91 (s, 6H, N(CH₃)₂, J_{Hpt} = 36.8 Hz), 2.25 (s, 3H, CH₃). ¹³C{¹H} NMR (150.9 MHz, CDCl₃): δ 134.01 (s, CH⁶, J_{CPt} = 82.7 Hz), 127.05 (s, CH⁵, J_{CPt} = 83.6 Hz), 122.65 (s, CH³, J_{CPt} = 52.4 Hz), 74.98 (s, CH₂N, J_{CPt} = 79.2 Hz), 52.36 (s, N(CH₃)₂), 46.92 (s, SCH₃, J_{CPt} = 95.1 Hz), 21.10 (s, CH₃). ¹⁹⁵Pt NMR (86.18 MHz, CDCl₃): δ -3677.19 (s). ESI-MS (pos. ion mode, CH₂Cl₂): *m/z* 421.09 ([M - Cl]⁺, calcd. 421.09).

Complex 6a. White solid. Yield: 43%. Anal. Calcd for **6a** C₁₁H₁₇BrClNOPtS: C, 25.32; H, 3.28; N, 2.68; S, 6.15. Found: C, 24.99; H, 3.19; N, 2.54; S, 6.05. ¹H NMR (400 MHz, CDCl₃): δ 8.11 (d, 1H, H⁶, J_{H6H4} = 1.6 Hz, J_{Hpt} = 52.0 Hz), 7.22 (dd, 1H, H⁴, J_{H4H3} = 8.0 Hz, J_{H4H6} = 1.6 Hz), 6.94 (d, 1H, H³, J_{H3H4} = 8.0 Hz), 3.94 (s, 2H, CH₂N, J_{Hpt} = 39.6 Hz), 3.54 (s, 6H, SCH₃, J_{Hpt} = 23.6 Hz), 2.91 (s, 6H, N(CH₃)₂, J_{Hpt} = 32.8 Hz). ¹³C{¹H} NMR (150.9 MHz, CDCl₃): δ 136.67 (s, CH⁶, J_{CPt} = 83.8 Hz), 127.89 (s, CH⁴), 123.24 (s, CH³), 74.55 (s, CH₂N, J_{CPt} = 77.0 Hz), 52.39 (s, N(CH₃)₂), 46.88 (s, SCH₃, J_{CPt} = 93.0 Hz). ¹⁹⁵Pt NMR (86.18 MHz, CDCl₃): δ -3624.38 (s). ESI-MS (pos. ion mode, CH₂Cl₂): *m/z* 485.99 ([M - Cl]⁺, calcd. 485.98).

Complex 7a. White solid. Yield: 30%. Anal. Calcd for **7a** C₁₁H₁₇BrClNOPtS: C, 25.32; H, 3.28; N, 2.74; S, 6.15. Found: C, 25.33; H, 3.27; N, 2.72; S, 6.15. ¹H NMR (400 MHz, CDCl₃): δ 7.82 (d, 1H, H⁶, J_{H6H5} = 8.4 Hz, J_{Hpt} = 46.0 Hz), 7.16 (m, 2H, H³+H⁵), 3.94 (s, 2H, CH₂N, J_{Hpt} = 40.0 Hz), 3.53 (s, 6H, SCH₃, J_{Hpt} = 23.6 Hz), 2.91 (s, 6H, N(CH₃)₂, J_{Hpt} = 32.4 Hz). ¹³C{¹H} NMR (150.9 MHz, CDCl₃): δ 136.08 (s, CH⁶, J_{CPt} = 85.7 Hz), 129.08 (s, CH⁵, J_{CPt} = 86.9 Hz), 124.71 (s, CH³, J_{CPt} = 57.8 Hz), 74.35 (s, CH₂N, J_{CPt} = 75.2 Hz), 52.43 (s, N(CH₃)₂), 46.91 (s, SCH₃, J_{CPt} = 93.7 Hz). ¹⁹⁵Pt NMR (86.18 MHz, CDCl₃): δ -3643.55 (s). ESI-MS (pos. ion mode, CH₂Cl₂): *m/z* 485.99 ([M - Cl]⁺, calcd. 485.98).

Complex 8a. White solid. Yield: 49%. Anal. Calcd for **8a** C₁₁H₁₇ClFNOPtS: C, 28.67; H, 3.72; N, 3.04; S, 6.96. Found: C, 28.72; H, 3.74; N, 3.05; S, 6.95. ¹H NMR (400 MHz, CDCl₃): δ 7.72 (dd, 1H, H⁶, J_{HF} = 11.2 Hz, J_{H6H4} = 2.8 Hz, J_{Hp} = 54 Hz), 7.03 (dd, 1H, H³, J_{H3H4} ≈ J_{HF} = 8.4 Hz), 6.76 (td, 1H, H⁴, J_{H4H3} ≈ J_{HF} = 8.4 Hz, J_{H4H6} = 2.8 Hz), 3.97 (s, 2H, CH₂N, J_{Hpt} = 39.6 Hz), 3.54 (s, 6H, SCH₃, J_{Hpt} = 24.0 Hz), 2.91 (s, 6H, N(CH₃)₂, J_{Hpt} = 33.6 Hz). ¹³C{¹H} NMR (150.9 MHz, CDCl₃): δ 122.56 (d, CH³, J_{CF} = 12.2 Hz), 119.60 (d, CH⁶, J_{CF} = 31.5 Hz), 111.50 (d, CH⁴, J_{CF} = 33.8 Hz),

74.48 (s, CH_2N), 52.37 (s, $\text{N}(\text{CH}_3)_2$), 46.88 (s, SCH_3 , $J_{\text{CPt}} = 92.4$ Hz). $^{19}\text{F}\{\text{H}\}$ NMR (282.40 MHz, CDCl_3): $\delta = -114.45$ (s, F, $J_{\text{FPt}} = 56.5$ Hz). ^{195}Pt NMR (86.18 MHz, CDCl_3): $\delta = -3630.71$ (s). ESI-MS (pos. ion mode, CH_2Cl_2): m/z 425.06 ($[\text{M} - \text{Cl}]^+$, calcd. 425.06).

Complex 9a. White solid. Yield: 57%. Anal. Calcd for **9a** $\text{C}_{11}\text{H}_{17}\text{ClFNOptS}$: C, 28.67; H, 3.72; N, 3.04; S, 6.96. Found: C, 28.70; H, 3.73; N, 3.01; S, 6.99. ^1H NMR (400 MHz, CDCl_3): δ 7.91 (dd, 1H, H^6 , $J_{\text{H}6\text{H}5} \approx J_{\text{HF}} = 8.4$ Hz, $J_{\text{HPt}} = 45.6$ Hz), 6.78 (m, 2H, H^3+H^5), 3.97 (s, 2H, CH_2N , $J_{\text{HPt}} = 39.6$ Hz), 3.55 (s, 6H, SCH_3 , $J_{\text{HPt}} = 2.4$ Hz), 2.93 (s, 6H, $\text{N}(\text{CH}_3)_2$, $J_{\text{HPt}} = 32.8$ Hz). $^{13}\text{C}\{\text{H}\}$ NMR (75.46 MHz, CDCl_3): δ 135.46 (s, CH^6 , $J_{\text{CPt}} = 36.2$ Hz), 112.55 (d, CH^5 , $J_{\text{CF}} = 19.2$ Hz, $J_{\text{CPt}} = 61$ Hz), 108.83 (d, CH^3 , $J_{\text{CF}} = 21.5$ Hz, $J_{\text{CPt}} = 61.6$ Hz), 74.32 (d, CH_2N , $J_{\text{CF}} = 2.5$ Hz, $J_{\text{CPt}} = 49$ Hz), 52.17 (s, $\text{N}(\text{CH}_3)_2$), 46.65 (s, SCH_3 , $J_{\text{CPt}} = 62.9$ Hz). $^{19}\text{F}\{\text{H}\}$ NMR (282.40 MHz, CDCl_3): $\delta = -118.56$ (s, F, $J_{\text{FPt}} = 11.3$ Hz). ^{195}Pt NMR (86.18 MHz, CDCl_3): $\delta = -3656.58$ (s). ESI-MS (pos. ion mode, CH_2Cl_2): m/z 425.06 ($[\text{M} - \text{Cl}]^+$, calcd. 425.06).

Complex 10a. White solid. Yield: 21%. Anal. Calcd for **10a** $\text{C}_{12}\text{H}_{17}\text{ClF}_3\text{NOPtS}$: C, 28.21; H, 3.35; N, 2.74; S, 6.28. Found: C, 28.25; H, 3.34; N, 2.72; S, 6.29. ^1H NMR (300 MHz, CDCl_3): δ 8.28 (s, 1H, H^6 , $J_{\text{HPt}} = 50.3$ Hz), 7.33 (d, 1H, H^4 , $J_{\text{H}4\text{H}3} = 7.8$ Hz), 7.14 (d, 1H, H^3 , $J_{\text{H}3\text{H}4} = 7.8$ Hz), 4.01 (s, 2H, CH_2N , $J_{\text{HPt}} = 39.6$ Hz), 3.55 (s, 6H, SCH_3 , $J_{\text{HPt}} = 24.9$ Hz), 2.93 (s, 6H, $\text{N}(\text{CH}_3)_2$, $J_{\text{HPt}} = 33.6$ Hz). $^{13}\text{C}\{\text{H}\}$ NMR (75.46 MHz, CDCl_3): δ 130.98 (s, CH^6), 121.51 (m, CH^3+CH^4), 74.74 (s, CH_2N , $J_{\text{CPt}} = 52.8$ Hz), 52.52 (s, $\text{N}(\text{CH}_3)_2$), 46.88 (s, SCH_3 , $J_{\text{CPt}} = 62.4$ Hz). $^{19}\text{F}\{\text{H}\}$ NMR (282.40 MHz, CDCl_3): $\delta = -62.18$ (s, CF_3). ^{195}Pt NMR (86.18 MHz, CDCl_3): $\delta = -3629.23$ (s). ESI-MS (pos. ion mode, CH_2Cl_2): m/z 475.06 ($[\text{M} - \text{Cl}]^+$, calcd. 425.06).

Complex 11a. White solid. Yield: 22%. Anal. Calcd for **11a** $\text{C}_{12}\text{H}_{17}\text{ClF}_3\text{NOPtS}$: C, 28.21; H, 3.35; N, 2.74; S, 6.28. Found: C, 28.22; H, 3.34; N, 2.72; S, 6.25. ^1H NMR (300 MHz, CDCl_3): δ 8.07 (m, 1H, H^6 , $J_{\text{HPt}} = 47.1$ Hz), 7.27 (m, 2H, H^3+H^5), 4.01 (s, 2H, CH_2N , $J_{\text{HPt}} = 40.5$ Hz), 3.55 (s, 6H, SCH_3 , $J_{\text{HPt}} = 24.9$ Hz), 2.92 (s, 6H, $\text{N}(\text{CH}_3)_2$, $J_{\text{HPt}} = 33.6$ Hz). $^{13}\text{C}\{\text{H}\}$ NMR (75.46 MHz, CDCl_3): δ 134.47 (s, CH^6 , $J_{\text{CPt}} = 54.3$ Hz), 122.60 (s, CH^5 , $J_{\text{CPt}} = 55.1$ Hz), 117.88 (s, CH^3 , $J_{\text{CPt}} = 21.1$ Hz), 74.42 (s, CH_2N , $J_{\text{CPt}} = 51.5$ Hz), 52.17 (s, $\text{N}(\text{CH}_3)_2$), 46.61 (s, SCH_3 , $J_{\text{CPt}} = 62.3$ Hz). $^{19}\text{F}\{\text{H}\}$ NMR (282.40 MHz, CDCl_3): $\delta = -62.21$ (s, CF_3). ^{195}Pt NMR (86.18 MHz, CDCl_3): $\delta = -3629.08$ (s). ESI-MS (pos. ion mode, CH_2Cl_2): m/z 475.06 ($[\text{M} - \text{Cl}]^+$, calcd. 425.06).

Complex 12a. Beige solid. Yield: 18%. Anal. Calcd for **12a** $\text{C}_{11}\text{H}_{17}\text{ClIn}_2\text{O}_3\text{PtS}$: C, 27.08; H, 3.51; N, 5.74; S, 6.57. Found: C, 27.10; H, 3.54; N, 5.72; S, 6.56. ^1H NMR (400 MHz, CDCl_3): δ 8.88 (d, 1H, H^6 , $J_{\text{H}6\text{H}4} = 2.4$ Hz, $J_{\text{HPt}} = 53.2$ Hz), 7.95 (dd, 1H, H^4 , $J_{\text{H}4\text{H}3} = 8.4$ Hz, $J_{\text{H}4\text{H}6} = 2.4$ Hz), 7.19 (d, 1H, H^3 , $J_{\text{H}3\text{H}4} = 8.4$ Hz), 4.05 (s, 2H, CH_2N , $J_{\text{HPt}} = 38.8$ Hz), 3.58 (s, 6H, SCH_3 , $J_{\text{HPt}} = 23.6$ Hz), 2.95 (s, 6H, $\text{N}(\text{CH}_3)_2$, $J_{\text{HPt}} = 32$ Hz). $^{13}\text{C}\{\text{H}\}$ NMR (150.9 MHz, CDCl_3): δ 128.90 (s, CH^6), 122.07 (s, CH^3), 120.18 (s, CH^4), 74.50 (s, CH_2N , $J_{\text{CPt}} = 75.5$ Hz), 52.59 (s, $\text{N}(\text{CH}_3)_2$), 46.83 (s, SCH_3 , $J_{\text{CPt}} = 91.3$ Hz). ^{195}Pt NMR (86.18 MHz, CDCl_3): $\delta = -3606.56$ (s). ESI-MS (pos. ion mode, CH_2Cl_2): m/z 452.06 ($[\text{M} - \text{Cl}]^+$, calcd. 452.06).

Complex 13a. Pale yellow solid. Yield: 14%. Anal. Calcd for **13a** $\text{C}_{11}\text{H}_{17}\text{ClIn}_2\text{O}_3\text{PtS}$: C, 27.08; H, 3.51; N, 5.74; S, 6.57. Found: C, 27.09; H, 3.54; N, 5.73; S, 6.58. ^1H NMR (400 MHz, CDCl_3): δ 8.16 (m, 1H, H^6 , $J_{\text{HPt}} = 46.4$ Hz), 7.89 (m, 2H, H^3+H^5), 4.06 (s, 2H, CH_2N , $J_{\text{HPt}} = 40.0$ Hz), 3.58 (s, 6H, SCH_3 , $J_{\text{HPt}} = 23.6$ Hz), 2.95 (s, 6H, $\text{N}(\text{CH}_3)_2$, $J_{\text{HPt}} = 32.8$ Hz). $^{13}\text{C}\{\text{H}\}$ NMR (150.9 MHz, CDCl_3): δ 135.05 (s, CH^6), 120.95 (s, CH^5), 116.28 (s, CH^3), 74.12 (s, CH_2N), 52.32 (s, $\text{N}(\text{CH}_3)_2$), 46.71 (s, SCH_3 , $J_{\text{CPt}} = 91.3$ Hz). ^{195}Pt NMR (86.18 MHz, CDCl_3): $\delta = -3587.25$ (s). ESI-MS (pos. ion mode, CH_2Cl_2): m/z 452.06 ($[\text{M} - \text{Cl}]^+$, calcd. 452.06).

General Procedure for the Synthesis of Cycloplatinated Phosphine Pt(II) Complexes 1b–13b. The platinum DMSO derivatives **1a–13a** was converted into the corresponding tris(4-trifluoromethyl-phenyl)phosphine derivatives **1b–13b** via ligand exchange.⁶⁰ These can also be prepared from the chloride dinuclear platinum complexes as we described previously.³⁰

Complex 2b. White solid. Yield: 73%. Anal. Calcd for **2b** $\text{C}_{31}\text{H}_{26}\text{ClF}_9\text{NOPPt}$: C, 43.24; H, 3.04; N, 1.63. Found: C, 43.25; H,

3.04; N, 1.64. ^1H NMR (400 MHz, CDCl_3): δ 7.86 (m, 6H, H_{ortho} PAr_3), 7.67 (d, 6H, H_{meta} PAr_3 , $J_{\text{HmHo}} = 7.6$ Hz), 7.01 (d, 1H, H^3 , $J_{\text{H}3\text{H}4} = 8.4$ Hz), 6.45 (dd, 1H, H^4 , $J_{\text{H}4\text{H}3} = 8.4$ Hz, $J_{\text{H}4\text{H}6} = 2.4$ Hz), 5.83 (d, 1H, H^6 , $J_{\text{H}6\text{H}4} = 2.4$ Hz, $J_{\text{HPt}} = 59.6$ Hz), 4.08 (d, 2H, CH_2N , $J_{\text{HPt}} = 2.4$ Hz, Pt satellites are observed as shoulders), 3.07 (s, 3H, OCH_3), 2.97 (d, 6H, $\text{N}(\text{CH}_3)_2$, $J_{\text{HPt}} = 2.8$ Hz, Pt satellites are observed as shoulders). $^{13}\text{C}\{\text{H}\}$ NMR (150.9 MHz, CDCl_3): δ 135.61 (d, CH_{ortho} PAr_3 , $J_{\text{CP}} = 17.4$ Hz), 125.32 (m, CH_{meta} PAr_3), 122.93 (s, CH^3), 122.81 (d, CH^6 , $J_{\text{CP}} = 9.8$ Hz), 109.94 (s, CH^4), 74.17 (s, CH_2N), 54.75 (s, OCH_3), 51.07 (s, $\text{N}(\text{CH}_3)_2$). $^{31}\text{P}\{\text{H}\}$ NMR (162.29 MHz, CDCl_3): δ 21.59 (s, $J_{\text{PPt}} = 4301.2$ Hz). $^{19}\text{F}\{\text{H}\}$ NMR (282.40 MHz, CDCl_3): $\delta = -63.08$ (s, CF_3 PAr_3). ^{195}Pt NMR (86.18 MHz, CDCl_3): $\delta = -4051.79$ (d, $J_{\text{PtP}} = 4301.2$ Hz). ESI-MS (pos. ion mode, CH_2Cl_2): m/z 825.13 ($[\text{M} - \text{Cl}]^+$, calcd. 825.13).

Complex 3b. White solid. Yield: 78%. Anal. Calcd for **3b** $\text{C}_{31}\text{H}_{26}\text{ClF}_9\text{NOPPt}$: C, 43.24; H, 3.04; N, 1.63. Found: C, 43.26; H, 3.03; N, 1.65. ^1H NMR (300 MHz, CDCl_3): δ 7.85 (m, 6H, H_{ortho} PAr_3), 7.65 (d, 6H, H_{meta} PAr_3 , $J_{\text{HmHo}} = 7.0$ Hz), 6.69 (d, 1H, H^3 , $J_{\text{HPt}} = 2.7$ Hz), 6.15 (dd, 1H, H^6 , $J_{\text{H}6\text{H}5} = 8.4$ Hz, $J_{\text{HPt}} = 3.0$ Hz, Pt satellites are observed as shoulders), 6.01 (dd, 1H, H^5 , $J_{\text{HS}H_6} = 8.4$ Hz, $J_{\text{HPt}} = 2.7$ Hz), 4.09 (d, 2H, CH_2N , $J_{\text{HPt}} = 3.0$ Hz, $J_{\text{HPt}} = 30.3$ Hz), 3.66 (s, 3H, OCH_3), 2.98 (d, 6H, $\text{N}(\text{CH}_3)_2$, $J_{\text{HPt}} = 3.0$ Hz, $J_{\text{HPt}} = 25.8$ Hz). $^{13}\text{C}\{\text{H}\}$ NMR (75.46 MHz, CDCl_3): δ 137.4 (d, CH^6 , $J_{\text{CP}} = 6.2$ Hz, $J_{\text{CPt}} = 86.5$ Hz), 135.32 (d, CH_{ortho} PAr_3 , $J_{\text{CP}} = 11.6$ Hz), 124.94 (m, CH_{meta} PAr_3), 110.77 (s, CH^5 , $J_{\text{CPt}} = 69.9$ Hz), 108.63 (s, CH^3), 74.42 (d, CH_2N , $J_{\text{CP}} = 3.2$ Hz, $J_{\text{CPt}} = 44.3$ Hz), 54.90 (s, OCH_3), 50.94 (s, $\text{N}(\text{CH}_3)_2$, $J_{\text{CPt}} = 2.5$ Hz). $^{31}\text{P}\{\text{H}\}$ NMR (162.29 MHz, CDCl_3): δ 21.66 (s, $J_{\text{PPt}} = 4355.6$ Hz). $^{19}\text{F}\{\text{H}\}$ NMR (282.40 MHz, CDCl_3): $\delta = -62.76$ (s, CF_3 PAr_3). ^{195}Pt NMR (86.18 MHz, CDCl_3): $\delta = -4093.11$ (d, $J_{\text{PtP}} = 4355.6$ Hz). ESI-MS (pos. ion mode, CH_2Cl_2): m/z 825.13 ($[\text{M} - \text{Cl}]^+$, calcd. 825.13).

Complex 4b. White solid. Yield: 14%. Anal. Calcd for **4b** $\text{C}_{31}\text{H}_{26}\text{ClF}_9\text{NPPt}$: C, 44.06; H, 3.10; N, 1.66. Found: C, 44.05; H, 3.11; N, 1.67. ^1H NMR (400 MHz, CDCl_3): δ 7.86 (m, 6H, H_{ortho} PAr_3), 7.66 (d, 6H, H_{meta} PAr_3 , $J_{\text{HmHo}} = 7.2$ Hz), 6.95 (d, 1H, H^3 , $J_{\text{H}3\text{H}4} = 7.6$ Hz), 6.69 (d, 1H, H^4 , $J_{\text{H}4\text{H}3} = 7.6$ Hz), 5.99 (s, 1H, H^6 , $J_{\text{HPt}} = 54.8$ Hz), 4.08 (d, 2H, CH_2N , $J_{\text{HPt}} = 2.8$ Hz, $J_{\text{HPt}} = 29.6$ Hz), 2.98 (d, 6H, $\text{N}(\text{CH}_3)_2$, $J_{\text{HPt}} = 2.8$ Hz, Pt satellites are observed as shoulders), 1.67 (s, 3H, CH_3). $^{13}\text{C}\{\text{H}\}$ NMR (75.46 MHz, CDCl_3): δ 138.0 (d, CH^6 , $J_{\text{CP}} = 5.6$ Hz), 135.44 (d, CH_{ortho} PAr_3 , $J_{\text{CP}} = 11.5$ Hz), 125.04 (m, CH_{meta} PAr_3), 124.35 (s, CH^4), 121.83 (s, CH^3), 74.34 (s, CH_2N), 50.92 (s, $\text{N}(\text{CH}_3)_2$), 20.80 (s, CH_3). $^{31}\text{P}\{\text{H}\}$ NMR (121.5 MHz, CDCl_3): δ 20.89 (s, $J_{\text{PPt}} = 4321.3$ Hz). $^{19}\text{F}\{\text{H}\}$ NMR (282.40 MHz, CDCl_3): $\delta = -63.17$ (s, CF_3 PAr_3). ^{195}Pt NMR (86.18 MHz, CDCl_3): $\delta = -4060.36$ (d, $J_{\text{PtP}} = 4321.3$ Hz). ESI-MS (pos. ion mode, CH_2Cl_2): m/z 809.13 ($[\text{M} - \text{Cl}]^+$, calcd. 809.13).

Complex 5b. White solid. Yield: 92%. Anal. Calcd for **5b** $\text{C}_{31}\text{H}_{26}\text{ClF}_9\text{NPPt}$: C, 44.06; H, 3.10; N, 1.66. Found: C, 44.08; H, 3.11; N, 1.64. ^1H NMR (400 MHz, CDCl_3): δ 7.81 (m, 6H, H_{ortho} PAr_3), 7.66 (d, 6H, H^3 , H_{meta} PAr_3 , $J_{\text{HmHo}} = 7.2$ Hz), 6.93 (s, 1H, H^3), 6.20 (m, 2H, H^5+H^6), 4.09 (d, 2H, CH_2N , $J_{\text{HPt}} = 2.8$ Hz, $J_{\text{HPt}} = 29.2$ Hz), 2.99 (d, 6H, $\text{N}(\text{CH}_3)_2$, Pt satellites are observed as shoulders), 2.13 (s, 3H, CH_3). $^{13}\text{C}\{\text{H}\}$ NMR (150.9 MHz, CDCl_3): δ 137.13 (d, CH^6 , $J_{\text{CP}} = 6.0$ Hz, $J_{\text{CPt}} = 86.0$ Hz), 135.62 (d, CH_{ortho} PAr_3 , $J_{\text{CP}} = 17.2$ Hz), 126.60 (s, CH^5 , $J_{\text{CPt}} = 69.0$ Hz), 125.22 (m, CH_{meta} PAr_3), 123.35 (s, CH^3), 74.72 (s, CH_2N), 51.19 (s, $\text{N}(\text{CH}_3)_2$), 21.00 (s, CH_3). $^{31}\text{P}\{\text{H}\}$ NMR (162.29 MHz, CDCl_3): δ 21.78 (s, $J_{\text{PPt}} = 4316.2$ Hz). $^{19}\text{F}\{\text{H}\}$ NMR (282.40 MHz, CDCl_3): $\delta = -62.77$ (s, CF_3 PAr_3). ^{195}Pt NMR (86.18 MHz, CDCl_3): $\delta = -4084.98$ (d, $J_{\text{PtP}} = 4316.2$ Hz). ESI-MS (pos. ion mode, CH_2Cl_2): m/z 809.13 ($[\text{M} - \text{Cl}]^+$, calcd. 809.13).

Complex 6b. White solid. Yield: 66%. Anal. Calcd for **6b** $\text{C}_{30}\text{H}_{23}\text{BrClF}_9\text{NPPt}$: C, 39.60; H, 2.55; N, 1.54. Found: C, 39.60; H, 2.61; N, 1.54. ^1H NMR (400 MHz, CDCl_3): δ 7.83 (m, 6H, H_{ortho} PAr_3), 7.69 (dd, 6H, H_{meta} PAr_3 , $J_{\text{HmHo}} = 8.0$ Hz, $J_{\text{HPt}} = 1.6$ Hz), 7.00 (dd, H^4 , $J_{\text{H}4\text{H}3} = 8.0$ Hz, $J_{\text{H}4\text{H}6} = 2.0$ Hz), 6.94 (d, 1H, H^3 , $J_{\text{H}3\text{H}4} = 8.0$ Hz), 6.23 (m, 1H, H^6 , $J_{\text{HPt}} = 57.6$ Hz), 4.05 (d, 2H, CH_2N , $J_{\text{HPt}} = 3.2$ Hz, Pt satellites are observed as shoulders). $^{13}\text{C}\{\text{H}\}$ NMR (150.9 MHz, CDCl_3): δ 139.06 (d, CH^6 , $J_{\text{CP}} = 8.9$ Hz), 135.56 (d, CH_{ortho} PAr_3 , $J_{\text{CP}} = 17.2$ Hz), 126.65 (s, CH^4), 125.43 (dd, CH_{meta} PAr_3 , $J_{\text{CP}} = 17.1$ Hz, $J_{\text{CF}} = 5.6$

Hz), 123.81 (s, CH³), 74.16 (d, CH₂N, *J*_{CP} = 5.0 Hz), 51.08 (d, N(CH₃)₂, *J*_{PPt} = 4.4 Hz). ³¹P{¹H} NMR (162.29 MHz, CDCl₃): δ 19.52 (s, *J*_{PPt} = 4250.7). ¹⁹F{¹H} NMR (282.40 MHz, CDCl₃): δ -63.16 (s, CF₃ PAr₃). ¹⁹⁵Pt NMR (86.18 MHz, CDCl₃): δ -4026.65 (d, *J*_{PPt} = 4250.7 Hz). ESI-MS (pos. ion mode, CH₂Cl₂): *m/z* 874.03 ([M - Cl]⁺, calcd. 874.02).

Complex 7b. White solid. Yield: 77%. Anal. Calcd for 7b C₃₀H₂₃BrClF₉NPPt: C, 39.60; H, 2.55; N, 1.54. Found: C, 39.58; H, 2.61; N, 1.58. ¹H NMR (400 MHz, CDCl₃): δ 7.83 (m, 6H, H_{ortho} PAr₃), 7.67 (dd, 6H, H_{meta} PAr₃, *J*_{HMHo} = 8.4 Hz, *J*_{HP} = 1.6 Hz), 7.21 (d, 1H, H³, *J*_{H3HS} = 2.4 Hz), 6.52 (dd, 1H, H⁵, *J*_{HSH6} = 8.4 Hz, *J*_{HSH3} = 2.4 Hz), 6.15 (dd, 1H, H⁶, *J*_{H6HS} = 8.4 Hz, *J*_{HP} = 3.2 Hz), 4.08 (d, 2H, CH₂N, *J*_{HPt} = 30.0 Hz, *J*_{HP} = 2.8 Hz), 2.98 (s, 6H, N(CH₃)₂, *J*_{HPt} = 28.8 Hz, *J*_{HP} = 2.8 Hz). ¹³C{¹H} NMR (150.9 MHz, CDCl₃): δ 138.55 (d, CH⁶, *J*_{CPt} = 121.32 Hz, *J*_{CP} = 9.2 Hz), 135.56 (d, CH_{ortho}, *J*_{CP} = 17.4 Hz), 128.77 (d, CH⁵, *J*_{CP} = 107.1 Hz, *J*_{CP} = 2.9 Hz), 125.37 (m, CH_{ortho}), 124.98 (s, CH³), 74.09 (d, CH₂N, *J*_{CP} = 4.7 Hz), 51.18 (d, N(CH₃)₂, *J*_{CP} = 3.2 Hz). ³¹P{¹H} NMR (162.29 MHz, CDCl₃): δ 21.02 (s, *J*_{PPt} = 4286.0 Hz). ¹⁹F{¹H} NMR (282.40 MHz, CDCl₃): δ -62.79 (s, CF₃ PAr₃). ¹⁹⁵Pt NMR (86.18 MHz, CDCl₃): δ -4058.34 (d, *J*_{PPt} = 4286.0 Hz). ESI-MS (pos. ion mode, CH₂Cl₂): *m/z* 874.03 ([M - Cl]⁺, calcd. 874.02).

Complex 9b. White solid. Yield: 71%. Anal. Calcd for 9b C₃₀H₂₃ClF₁₀NPPt: C, 42.44; H, 2.73; N, 2.68. Found: C, 43.54; H, 2.70; N, 2.66. ¹H NMR (300 MHz, CDCl₃): δ 7.84 (m, 6H, H_{ortho} PAr₃), 7.66 (dd, 6H, H_{meta} PAr₃, *J*_{HMHo} = 8.1 Hz, *J*_{HP} = 1.5 Hz), 6.82 (dd, 1H, H³, *J*_{HF} = 9.3 Hz, *J*_{H3HS} = 2.4 Hz), 6.16 (m, 2H, H⁶+H⁵), 4.09 (d, 2H, CH₂N, *J*_{HP} = 3.0 Hz, *J*_{HPt} = 31.2 Hz), 2.98 (d, 6H, N(CH₃)₂, *J*_{HP} = 3.0 Hz, *J*_{HPt} = 26.1 Hz). ¹³C{¹H} NMR (75.46 MHz, CDCl₃): δ 137.65 (m, CH⁶, *J*_{CPt} = 78.0 Hz), 135.29 (d, CH_{meta} PAr₃, *J*_{CP} = 11.5 Hz), 125.04 (m, CH_{ortho} PAr₃), 112.34 (d, CH⁵, *J*_{CP} = 19.5 Hz), 109.51 (d, CH³, *J*_{CP} = 20.9 Hz), 74.06 (s, CH₂N, *J*_{CP} = 50.9 Hz), 50.88 (s, N(CH₃)₂). ³¹P{¹H} NMR (112.5 MHz, CDCl₃): δ 21.07 (s, *J*_{PPt} = 4273.3 Hz). ¹⁹F{¹H} NMR (282.40 MHz, CDCl₃): δ -62.79 (s, CF₃ PAr₃), -119.41 (s, F, *J*_{FPt} = 11.3 Hz). ¹⁹⁵Pt NMR (86.18 MHz, CDCl₃): δ -4073.41 (d, *J*_{PPt} = 4273.3 Hz). ESI-MS (pos. ion mode, CH₂Cl₂): *m/z* 813.11 ([M - Cl]⁺, calcd. 813.11).

Complex 11b. White solid. Yield: 13%. Anal. Calcd for 11b C₃₁H₂₃ClF₁₂NPPt: C, 41.42; H, 2.58; N, 1.56. Found: C, 41.45; H, 2.54; N, 1.57. ¹H NMR (400 MHz, CDCl₃): δ 7.83 (m, 6H, H_{ortho} PAr₃), 7.67 (dd, H_{meta} PAr₃, *J*_{HMHo} = 8.0 Hz, *J*_{HP} = 1.6 Hz), 7.30 (d, 1H, H³, *J*_{HP} = 1.2 Hz), 6.65 (dd, 1H, H⁵, *J*_{HSH6} = 8.0 Hz, *J*_{HP} = 1.2 Hz), 6.40 (dd, 1H, H⁶, *J*_{H6HS} = 8.0 Hz, *J*_{HP} = 2.9 Hz, *J*_{HPt} = 49.5 Hz), 4.15 (d, 2H, CH₂N, *J*_{HP} = 2.8 Hz, *J*_{HPt} = 49.5 Hz), 2.99 (d, 6H, N(CH₃)₂, *J*_{HP} = 2.8 Hz, *J*_{HPt} = 27.6 Hz). ¹³C{¹H} NMR (150.9 MHz, CDCl₃): δ 136.95 (d, CH⁶, *J*_{CP} = 9.4 Hz, *J*_{CPt} = 134.6 Hz), 135.35 (d, CH_{ortho} PAr₃, *J*_{CP} = 17.2 Hz), 125.22 (m, CH_{meta} PAr₃), 122.33 (d, CH⁵, *J*_{CPt} = 100.2 Hz), 118.69 (d, CH³, *J*_{CP} = 5.3 Hz), 74.19 (d, CH₂N, *J*_{CP} = 4.8 Hz, *J*_{CPt} = 69.4 Hz), 51.00 (d, N(CH₃)₂, *J*_{CP} = 3.8 Hz). ³¹P{¹H} NMR (162.29 MHz, CDCl₃): δ 20.80 (s, *J*_{PPt} = 4232.1 Hz). ¹⁹F{¹H} NMR (282.40 MHz, CDCl₃): δ -62.34 (s, CF₃), -63.18 (s, CF₃ PAr₃). ¹⁹⁵Pt NMR (86.18 MHz, CDCl₃): δ -4036.40 (d, *J*_{PPt} = 4232.1 Hz). ESI-MS (pos. ion mode, CH₂Cl₂): *m/z* 863.10 ([M - Cl]⁺, calcd. 863.10).

Complex 12b. Beige solid. Yield: 71%. Anal. Calcd for 12b C₃₀H₂₃ClN₂O₂PPt: C, 41.13; H, 2.65; N, 3.20. Found: C, 41.15; H, 2.68; N, 3.32. ¹H NMR (400 MHz, CDCl₃): δ 7.84 (m, 6H, H_{ortho} PAr₃), 7.75 (dd, 1H, H⁴, *J*_{H4H3} = 8.4 Hz, *J*_{H4H6} = 2.4 Hz), 7.68 (dd, 6H, H_{meta} PAr₃, *J*_{HMHo} = 8.4 Hz, *J*_{HP} = 1.6 Hz), 7.19 (d, 1H, H³, *J*_{H3H4} = 8.4 Hz), 7.14 (m, 1H, H⁶, *J*_{HPt} = 59.2 Hz), 4.15 (d, 2H, CH₂N, *J*_{HP} = 3.2 Hz, *J*_{HPt} = 28.4 Hz), 2.99 (d, 6H, N(CH₃)₂, *J*_{HP} = 3.2 Hz, *J*_{HPt} = 27.2 Hz). ¹³C{¹H} NMR (150.9 MHz, CDCl₃): δ 135.40 (d, CH_{ortho} PAr₃, *J*_{CP} = 17.1 Hz), 130.85 (d, CH⁶, *J*_{CP} = 9.8 Hz), 125.56 (m, CH_{meta} PAr₃), 122.72 (s, CH³), 119.09 (s, CH⁴), 74.19 (d, CH₂N, *J*_{CP} = 5.0 Hz), 51.25 (d, N(CH₃)₂, *J*_{CP} = 4.1 Hz). ³¹P{¹H} NMR (162.29 MHz, CDCl₃): δ 19.55 (s, *J*_{PPt} = 4187.5 Hz). ¹⁹F{¹H} NMR (282.40 MHz, CDCl₃): δ -63.13 (s, CF₃ PAr₃). ¹⁹⁵Pt NMR (86.18 MHz, CDCl₃): δ -4009.12 (d, *J*_{PPt} = 4187.5 Hz). ESI-MS (pos. ion mode, CH₂Cl₂): *m/z* 840.10 ([M - Cl]⁺, calcd. 840.10).

Complex 13b. Yellow solid. Yield: 62%. Anal. Calcd for 13b C₃₀H₂₃ClF₉N₂O₂PPt: C, 41.13; H, 2.65; N, 3.20. Found: C, 41.16; H,

2.68; N, 3.12. ¹H NMR (300 MHz, CDCl₃): δ 7.91 (d, 1H, H³, *J*_{HP} = 2.7 Hz), 7.82 (m, 6H, H_{ortho} PAr₃), 7.68 (dd, 6H, H_{meta} PAr₃, *J*_{HMHo} = 8.4 Hz, *J*_{HP} = 1.8 Hz), 7.27 (dd, 1H, H⁵, *J*_{HSH6} = 8.4 Hz, *J*_{HP} = 2.7 Hz), 6.45 (dd, 1H, H⁶, *J*_{H6HS} = 8.4 Hz, *J*_{HP} = 2.7 Hz, *J*_{HPt} = 54 Hz), 4.19 (d, 2H, CH₂N, *J*_{HP} = 3.0 Hz, *J*_{HPt} = 31.5 Hz), 3.58 (s, 6H, SCH₃, *J*_{HPt} = 23.6 Hz), 2.99 (d, 6H, N(CH₃)₂, *J*_{HP} = 3.3 Hz, *J*_{HPt} = 26.4 Hz). ¹³C{¹H} NMR (75.46 MHz, CDCl₃): δ 137.58 (d, CH⁶, *J*_{CP} = 6.3 Hz), 135.79 (d, CH_{ortho} PAr₃, *J*_{CP} = 11.5 Hz), 125.84 (m, CH_{meta} PAr₃), 121.22 (s, CH⁵), 117.47 (s, CH³), 74.29 (d, CH₂N, *J*_{CP} = 3.2 Hz), 51.51 (s, N(CH₃)₂, *J*_{CP} = 2.4 Hz). ³¹P{¹H} NMR (112.5 MHz, CDCl₃): δ 20.23 (s, *J*_{PPt} = 4193.6 Hz). ¹⁹F{¹H} NMR (282.40 MHz, CDCl₃): δ -62.83 (s, CF₃ PAr₃). ¹⁹⁵Pt NMR (86.18 MHz, CDCl₃): δ -3986.71 (d, *J*_{PPt} = 4193.6 Hz). ESI-MS (pos. ion mode, CH₂Cl₂): *m/z* 840.10 ([M - Cl]⁺, calcd. 840.10).

X-ray Crystal Structure Analysis. Single crystals suitable for X-ray diffraction analysis were obtained for complexes 8a and 2b from CH₂Cl₂/toluene/hexane. A summary of crystal data collection and refinement parameters for all compounds are given in Tables S1–S6 in the Supporting Information. Crystals were mounted on glass fibers and transferred to the cold gas stream of the diffractometer Bruker Smart APEX. Data were recorded with Mo K α radiation (λ = 0.71073 Å) in ω scan mode. Absorption correction for the compound was based on multiscans.

Both structures were solved by direct methods (SHELXS-97),⁶¹ refinement was done by full-matrix least-squares on F^2 using the SHELXL-97 program suite,⁶¹ and empirical (multiscan) absorption correction was performed with SADABS (Bruker).⁶² All non-hydrogen positions were refined with anisotropic temperature factors. Hydrogen atoms for aromatic CH and aliphatic CH₂ and CH₃ groups were positioned geometrically (C-H = 0.95 Å for aromatic CH, C-H = 0.99 Å for CH₂, C-H = 0.98 Å for CH₃) and refined using a riding model (AFIX 43 for aromatic CH, AFIX 23 for CH₂, AFIX 137 for CH₃), with U_{iso} (H) = 1.2 U_{eq} (CH, CH₂) and U_{iso} (H) = 1.5 U_{eq} (CH₃). Graphics were drawn with DIAMOND (Version 3.2).⁶³

Cell Lines and Culture Conditions. Human ovarian carcinoma A2780 and A2780cisR cell lines were grown in RPMI-1640, supplemented with 10% (v/v) final concentration heat-inactivated fetal bovine serum (FBS, Sigma, USA), 2 mM L-glutamine, and antibiotics (penicillin/streptomycin). Both cell lines were maintained at 310 K in humidified atmosphere containing 5% CO₂. In order to retain resistance to CDDP, A2780cisR was added to every two subcultures.

The nontumorigenic BGM cells (African green monkey kidney) were grown in dubecco's modified eagle's medium (DMEM) without phenol red to contain 1 g/L glucose supplemented with 10% (v/v) final concentration heat-inactivated FBS, 2 mM L-glutamine, 2 mM sodium pyruvate, and antibiotics (penicillin/streptomycin) at 310 K in humidified atmosphere containing 7.5%–10% CO₂.

Ovarian carcinoma cell line was obtained from European Collection of Animal Cell Culture (ECACC, Salisbury, U.K.). BGM and EA.hy926 lines were obtained from American Tissue Culture Collection (ATCC, U.S.A.).

Before and after experiments, all cell lines were mycoplasma-free, as the Hoechst DNA stain method determined.⁶⁴

Cells from 80% confluent monolayers were removed from flasks by 0.25% trypsin solution (Sigma-Aldrich), centrifuged at 200g 10', washed twice with PBS, and pellet diluted with complete medium. Medium was changed twice per week.

Cytotoxicity Assays. Cell proliferation was evaluated by MTT assay, (3-(4,5-dimethylthiazol-2-yl)-2,5-diphenyltetrazolium bromide. A2780, A2780cisR, BGM, and EA.hy926 were plated in 96-well sterile plates at a density of 5×10^3 cells/well with 200 μ L of medium and were then incubated for 24 h. After attachment to the culture surface, cells were incubated with various concentrations of the compounds tested freshly dissolved in DMSO and diluted in the culture medium (DMSO final concentration 0.4%) for 48 h at 310 K. For MTT assay, the medium was removed by pipetting and then 200 μ L of corresponding medium for each cell line was added and 50 μ L of a MTT solution 5 mg/mL was added and left at 310 K for 4 h in the dark. Finally, this solution was removed from each plate, and 100 μ L of

DMSO was added and shook 5 min at 120 rpm (always at dark) before measurement. Absorbance was measured at 560 nm for MTT assays in a Fluorstar Omega spectrophotometer. The effects of complexes were expressed as corrected percentage inhibition values according to the following equation,

$$\% \text{inhibition} = \left[1 - \left(\frac{T}{C} \right) \right] \times 100$$

where T is the mean absorbance of the treated cells and C the mean absorbance in the controls.

The inhibitory potential of compounds was measured by calculating concentration-percentage inhibition curves; these curves were adjusted to the following equation:

$$E = \frac{E_{\max}}{1 + \left(\frac{IC_{50}}{C} \right)^n}$$

where E is the percentage inhibition observed, E_{\max} is the maximal effects, IC_{50} is the concentration that inhibits 50% of maximal growth, C is the concentration of compounds tested and n is the slope of the semilogarithmic dose-response sigmoid curves. This nonlinear fitting was performed using Sigma Plot 11.0 software.

For comparison purposes, the cytotoxicity of CDDP was evaluated under the same experimental conditions. All compounds were tested in three independent studies with quadruplicate points. The *in vitro* studies were performed in the SACE service (Support Service for Experimental Sciences, University of Murcia, Murcia, Spain).

All studies were performed with maximum DMSO concentration of 0.4% (except for cisplatin, water diluted) and in all the experiments measurements were corrected with a water control.

TEM Sample Preparations. One million cells/well were cultured a 6-well plate and left for 24 h at 310 K. Afterward, 1 μ M of **1a** and **8a** and 4 μ M of **2b** was added and left again for 24 h at the same temperature. The medium was then added to a Falcon tube. Cells were removed from the wells with trypsin and the resulting suspension put together in the Falcon tube with the medium. Centrifugation (200g, 10 min) was followed, discarding the supernatant. Cells were fixed with glutaraldehyde (2.50%) for 1.5 h and then washed with cacodilate buffer by means of centrifugation (same conditions). Then, addition of ethanol at increasing concentrations (30, 50, 70, 90%) for 10 min was added to the cells. Subsequently, absolute ethanol and, at the same time, copper(II) sulfate for 10 min were added. Then, complete dehydration was achieved by subsequent additions of propylene oxide in epoxy resins at higher concentrations and delays. Finally, the capsules were left in the epoxy resin for a complete night and cut to micrometer dimensions, and 70–80 nm sections were collected on copper grids. The sections were imaged on a ZEIS EM10 TEM. Neither osmium tetroxide nor uranyl acetate were added during this process to ensure that contrast images were only due to the added metal drug.

Cell Cycle Arrest Assays. Cell cycle arrest studies were performed on A2780 and A2780cisR ovarian cancer cells. Typically, 1.5×10^5 cells were seeded in a 6-well plate with RPMI medium (5 mL/plate). Cells were allowed to fix to the plate by incubation for 24 h at 310 K (5% CO₂). Then, the compounds were added at final concentrations similar to their respective IC₅₀ values in the different plates. One well for each line was untreated, for being used as a control. The cultures were incubated for other additional 24 h in the same conditions as described above. At this point, the medium was removed and stored in 15 mL Falcon tubes. Immediately, the fixed cells were treated with 1 mL of trypsin for 4 min at 310 K and then 1 mL of RPMI medium containing FBS was added to stop the enzymatic action. The resulting 2 mL were added to the 15 mL Falcon tubes. In this way both possible floating cells and adherent cells were considered for the assay. Cells were centrifuged (250g, 10 min) and the precipitated cells were washed with 2 mL of PBS. After another centrifugation in same conditions, removed the supernatant, cells were resuspended in 200 μ L of PBS. Subsequently, 1 mL of a PBS (30%)/ethanol (70%) mix solution was added to the cells. The solution was kept in ice for 30

min. The supernatant was eliminated by centrifugation (same conditions). The cells were again resuspended with 800 μ L of PBS. Finally, 100 μ L of RNase solution (1 mg/mL) and 100 μ L of propidium iodide solution (400 μ g/mL) were added. After stirring the resulting suspension was incubated at 310 K for 30 min at dark. Stained cells were analyzed in a Becton-Dickinson FACScalibur flow cytometer. In each case 30000 events were acquired.

Apoptosis Experiments. For apoptosis determination assays, 1.5×10^5 cells were typically seeded in a 6-well plate. Ovarian cancer cells with compounds and their control were incubated, collected and washed twice with PBS as described above (no PBS/Ethanol mix was used in this case). After removing the PBS, 40 μ L of a solution containing Annexin V and PI (Annexin-V-Fluos from Roche) and 160 μ L of incubation buffer (hepes 10 mM, NaCl 140 mM, CaCl₂ 5 mM pH = 7.4) was added to the cell pellet. Cells were resuspended in this solution and left at room temperature in dark for 15 min 200 μ L of PBS was added immediately previous to the measurements. These were carried out in a Beckman Coulter Epics XL flow cytometer, registering the emission at wavelengths of 620 and 525 nm for PI and Annexin V, respectively. In each case, 10000 events were acquired.

Platinum Cellular Accumulation Studies. Ovarian cancer cells were plated in a 6-well cell culture plate at a density of 10^6 cells/well and maintained at 310 K in a 5% CO₂ atmosphere. Compounds **4a**, **4b**, and CDDP were added to cells for 24 h at IC₅₀ concentration, respectively. After this time, cells were harvested from the plate by using EDTA-Trypsin. An Aliquot of cell suspension was lysed in buffer containing 1% SDS, 150 mM NaCl, 20 mM HEPES, 1 mM EDTA, 0.5% Triton X-100, 1 mM Na₂VO₄, and 1% protease inhibitor mix before sonication. Lysates were centrifuged for 5 min at 278 K and 20.000g to separate the proteins extracts from insoluble cell debits. Total protein content was estimated by a DC assay (Bio-Rad). Cell suspension from each well was transferred to eppendorf tubes and centrifuged at 400g for 5 min at room temperature. The supernatant was discarded and pellet was centrifuged in a vacuum-dry evaporator centrifuge for 1 h. Evaporated samples were resuspended with 200 μ L subboiled 65% HNO₃ (Subboiled suprapur 65% nitric acid, Merck) and 50 μ L H₂O₂ and transferred to the microwave container. The eppendorf tubes were cleaned with 250 μ L subboiled 65% HNO₃ in order to transfer the whole sample. The samples were digested for 10 min at 60% capacity. The vials were allowed to cool, opened and 1.5 mL concentrated (30%) HCl was added to each vial. The samples were again digested for 10 min at 60% capacity and filtrated afterward with a 0.45 μ m filter. Same process was made with blank (acid only) as a control. Total digested cells were transferred to a 5 mL measuring flask and diluted with acid mix (0.65% HNO₃ and 1.0% HCl). Microwave containers were cleaned with acid mix in order to transfer the whole sample before analysis ICP-MS.

A PerkinElmer Sciex Elan 6000 DRC-e ICP-MS instrument (PerkinElmer, Norwalk, CT) equipped with a water cooled cyclonic spray chamber maintained at 277 K and a micromist nebulizer (both from Glass Expansion, Melbourne, Australia) was used to determine Pt concentration. Pt was monitored, and ¹⁹⁴Pt and ¹⁹⁵Pt isotopes were used as internal standards. The instrument sensitivity was approximately 14000 cps/ppb Pt, and the detection limit was estimated to be 0.01 μ g/L Pt.

Samples were introduced via a concentric glass nebulizer with a free aspiration rate of 0.2 mL/min, a Peltier-cooled double pass glass spray chamber, and a quartz torch. A peristaltic pump carried samples from a SPS3 autosampler (Varian) to the nebulizer. Pt standards were prepared by serial dilution of a solution containing 10 mg/L of Pt in 5% HCl (Trace Cert. Fluka). Twelve calibration curve was made over a concentration range of 0.075–5 μ g/L. Data acquisition was done using peak hopping with a dwell time of 30 ms, 25 scans/5 replicate, and three replicates per sample from two independent experiments. The graph was done with the GraphPad Prism 5 software.

Reactions of the Complexes with 9-Ethylguanine Followed by ¹H NMR. 9-Ethylguanine was incubated with the complexes in a 5:1 ratio in an NMR tube containing D₂O:DMSO-*d*₆ (1:4) as solvent. The final concentration of complexes in the NMR tube was 1.0 mM. The reaction was followed for 24 h at 310 K.

Hoechst 33258 Displacement Experiments. 3 mL of a solution, that is, 20 μM DNA and 2 μM Hoechst 33258 in Tris buffer was titrated with aliquots of a concentrated solution of the complex, producing solutions with varied mole ratios of complex to ct-DNA. After each addition the solution was stirred at the appropriate temperature for 5 min before measurement. The fluorescence spectra of the solution were obtained by exciting at 338 nm and measuring the emission spectra from 350–650 nm (with $\lambda_{\text{max}} \sim 600$ nm) using 5 nm slits.

Endothelial Tube Formation Assay. Unpolymerized matrigel (8.7 mg/mL; B&D Biosciences, Bedford, MA) was placed in 96-well plates (9 μL /well) and allowed to polymerize for 1 h at 310 K. This study revealed that tube formation was maximal after 12 h at the concentration of 12×10^3 cells/well for EA.hy926). EA.hy926 cells were suspended in medium without FBS at different concentrations of each compound **1a–13a**. The cells were seeded on top of the matrigel layer and incubated at 310 K. After 12 h for EA.hy926 cells, the wells were photographed using an inverted phase-contrast microscope (Nikon mod. Eclipse TE-2000-U). EA.hy926 cells formed capillary-like networks with different tube morphology. Tube formation was quantified by measuring the total length of the tube network, number of network, and area of network under 4 \times magnification using ImageJ software (National Institutes of Health, Bethesda, MD, USA).

Wound Assay (Migration). EA.hy926 cells were cultured as confluent monolayers in 96-well plates, synchronized in 1% FBS for 24 h and wounded by removing strip of cells across the well with a standard 200 μL pipet tip. Wounded monolayers were washed twice with PBS to remove nonadherent cells and then treated with compounds **1a–13a** for 8 h. EA.hy926 cell migration was recorded under inverted microscope (Nikon mod. Eclipse TE-2000-U). Wound healing was quantified,⁵⁷ using ImageJ Software (National Institutes of Health, Bethesda, MD, USA), as follows: Wound healing area (%) = [cell-free area (0 h) – cell-free area (8 h)]/cell-free area (0 h) \times 100.

Statistical Analysis. The nonparametric Kruskal–Wallis test was used to compare multiple independent groups of numerical data. If the test was significant, U-Mann–Whitney tests were applied to compare each experimental condition to the control. All statistical analyses were performed using PASW Statistics 18.

■ ASSOCIATED CONTENT

Supporting Information

Additional crystallographic data, figures for cell cycle analysis, apoptosis, Hoechst 33258 displacement experiment, inhibited tube formation images; **4a** and **4b** ^1H NMR spectra; and low-field region of the ^1H NMR spectra of complexes **8a** and **2b** reactions with 9-EtG. This material is available free of charge via the Internet at <http://pubs.acs.org>.

■ AUTHOR INFORMATION

Corresponding Author

*E-mail: jruiz@um.es. Fax: +34 868 884148. Tel: +34 868 887455.

Notes

The authors declare no competing financial interest.

■ ACKNOWLEDGMENTS

This work was supported by the Spanish Ministerio de Economía y Competitividad and FEDER (Project SAF2011-26611) and by Fundación Séneca-CARM (Projects 08666/PI/08 and 15354/PI/10). A.Z. thanks Fundación Séneca-CARM for a grant (Exp. 19020/FPI/13). G.S.Y. thanks the European Union Seventh Framework Programme—Marie Curie Cofund (FP7/2007–2013) under U-IMPACT Grant Agreement 267143, COST CM1105 for providing opportunities for discussion, and Dr. Ian Lambert, Dr. Stephan Stürup, and

Celina StØving Dam for their collaboration on the platinum accumulation experiment.

■ ABBREVIATIONS USED

A2780, ovarian cancer cell line; A2780cisR, cisplatin resistant ovarian cancer cell line; BGM, healthy kidney cell line from African green monkey; CDDP, cisplatin; dmiba, dimethylbenzylamine; DMEM, dubelcco's modified eagle's medium; DMSO, dimethyl sulfoxide; EA.hy926, endothelial cell line; EDTA, ethylenediaminetetraacetic acid; EHS, Engelbreth–Holm–Swarm; 9-EtG, 9-ethylguanine; FACS, fluorescence activated cell sorter; FBS, fetal bovine serum; GSH, glutathione; MTT, 3-(4,5-dimethylthiazol-2-yl)-2,5-diphenyltetrazolium bromide; PBS, phosphate buffer saline; PI, propidium iodide; PS, phosphatidylserine; RF, resistance factor; RPMI, Roswell Park Memorial Institute medium; SF, selectivity factor; TEM, transmission electron microscopy; VEGFR3, vascular endothelial grow factor receptor 3

■ REFERENCES

- (1) *Cancer Facts & Figures 2013*; American Cancer Society: Atlanta, 2013; pp 1–60.
- (2) Muggia, F. Platinum compounds 30 years after the introduction of cisplatin: Implications for the treatment of ovarian cancer. *Gynecol. Oncol.* **2009**, *112*, 275–281.
- (3) Schmid, B. C.; Oehler, M. K. New perspectives in ovarian cancer treatment. *Maturitas* **2014**, *77*, 128–136.
- (4) Ma, J.; Waxman, D. J. Combination of antiangiogenesis with chemotherapy for more effective cancer treatment. *Mol. Cancer Ther.* **2008**, *7*, 3670–3684.
- (5) Teoh, D. G.; Secord, A. A. Antiangiogenic therapies in epithelial ovarian cancer. *Cancer Control* **2011**, *18*, 31–43.
- (6) Barry, N. P. E.; Sadler, P. J. Exploration of the medical periodic table: towards new targets. *Chem. Commun.* **2013**, *49*, 5106–5131.
- (7) Patra, M.; Gasser, G. Organometallic compounds: an opportunity for chemical biology? *ChemBioChem* **2012**, *13*, 1232–1252.
- (8) Cutillas, N.; Yello, G. S.; de Haro, C.; Vicente, C.; Rodríguez, V.; Ruiz, J. Anticancer cyclometalated complexes of platinum group metals and gold. *Coord. Chem. Rev.* **2013**, *257*, 2784–2797.
- (9) Chow, M. J.; Licona, C.; Yuan Qiang Wong, D.; Pastorin, G.; Gaiddon, C.; Ang, W. H. Discovery and investigation of anticancer ruthenium–arene schiff-base complexes via water-promoted combinatorial three-component assembly. *J. Med. Chem.* **2014**, *57*, 6043–6059.
- (10) Gasser, G.; Ott, I.; Metzler-Nolte, N. Organometallic anticancer compounds. *J. Med. Chem.* **2010**, *54*, 3–25.
- (11) Liu, W.; Gust, R. Metal N-heterocyclic carbene complexes as potential antitumor metallodrugs. *Chem. Soc. Rev.* **2013**, *42*, 755–773.
- (12) Zou, T.; Lok, C.-N.; Fung, Y. M. E.; Che, C.-M. Luminescent organoplatinum(II) complexes containing bis(N-heterocyclic carbene) ligands selectively target the endoplasmic reticulum and induce potent photo-toxicity. *Chem. Commun.* **2013**, *49*, 5423–5425.
- (13) Ma, D.-L.; He, H.-Z.; Leung, K.-H.; Chan, D. S.-H.; Leung, C.-H. Bioactive luminescent transition-metal complexes for biomedical applications. *Angew. Chem., Int. Ed.* **2013**, *52*, 7666–7682.
- (14) Suntharalingam, K.; Łęczkowska, A.; Furrer, M. A.; Wu, Y.; Kuimova, M. K.; Therrien, B.; White, A. J. P.; Vilar, R. A cyclometallated platinum complex as a selective optical switch for quadruplex DNA. *Chem.—Eur. J.* **2012**, *18*, 16277–16282.
- (15) Ma, D.-L.; Che, C.-M.; Yan, S.-C. Platinum(II) complexes with dipyridophenazine ligands as human telomerase inhibitors and luminescent probes for G-quadruplex DNA. *J. Am. Chem. Soc.* **2008**, *131*, 1835–1846.
- (16) Wai-Yin Sun, R.; Lok-Fung Chow, A.; Li, X.-H.; Yan, J. J.; Sin-Yin Chui, S.; Che, C.-M. Luminescent cyclometalated platinum(II) complexes containing N-heterocyclic carbene ligands with potent in vitro and in vivo anti-cancer properties accumulate in cytoplasmic structures of cancer cells. *Chem. Sci.* **2011**, *2*, 728–736.

- (17) Rademaker-Lakhai, J. M.; van den Bongard, D.; Pluim, D.; Beijnen, J. H.; Schellens, J. H. A Phase I and pharmacological study with imidazolium-trans-DMSO-imidazole-tetrachlororuthenate, a novel ruthenium anticancer agent. *Clin. Cancer Res.* **2004**, *10*, 3717–3727.
- (18) Yang, L.; Zhang, J.; Wang, C.; Qin, X.; Yu, Q.; Zhou, Y.; Liu, J. Interaction between 8-hydroxyquinoline ruthenium(II) complexes and basic fibroblast growth factors (bFGF): inhibiting angiogenesis and tumor growth through ERK and AKT signaling pathways. *Metalomics* **2014**, *6*, 518–531.
- (19) Nowak-Sliwinska, P.; van Beijnum, J. R.; Casini, A.; Nazarov, A. A.; Wagnières, G.; van den Bergh, H.; Dyson, P. J.; Griffioen, A. W. Organometallic ruthenium(II) arene compounds with antiangiogenic activity. *J. Med. Chem.* **2011**, *54*, 3895–3902.
- (20) Liu, L.-J.; Lin, S.; Chan, D. S.-H.; Vong, C. T.; Hoi, P. M.; Wong, C.-Y.; Ma, D.-L.; Leung, C.-H. A rhodium(III) complex inhibits LPS-induced nitric oxide production and angiogenic activity in cellulo. *J. Inorg. Biochem.* **2014**, *140*, 23–28.
- (21) Wilbuer, A.; Vlecken, D. H.; Schmitz, D. J.; Kräling, K.; Harms, K.; Bagowski, C. P.; Meggers, E. Iridium complex with antiangiogenic properties. *Angew. Chem., Int. Ed.* **2010**, *49*, 3839–3842.
- (22) Feng, L.; Geisselbrecht, Y.; Blanck, S.; Wilbuer, A.; Atilla-Gokcumen, G. E.; Filippakopoulos, P.; Kräling, K.; Celik, M. A.; Harms, K.; Maksimoska, J.; Marmorstein, R.; Frenking, G.; Knapp, S.; Essen, L.-O.; Meggers, E. Structurally sophisticated octahedral metal complexes as highly selective protein kinase inhibitors. *J. Am. Chem. Soc.* **2011**, *133*, 5976–5986.
- (23) Clavel, C. M.; Păunescu, E.; Nowak-Sliwinska, P.; Griffioen, A. W.; Scopelliti, R.; Dyson, P. J. Discovery of a highly tumor-selective organometallic ruthenium(II)–arene complex. *J. Med. Chem.* **2014**, *57*, 3546–3558.
- (24) Nazarov, A. A.; Baquié, M.; Nowak-Sliwinska, P.; Zava, O.; van Beijnum, J. R.; Groessl, M.; Chisholm, D. M.; Ahmadi, Z.; McIndoe, J. S.; Griffioen, A. W.; van den Bergh, H.; Dyson, P. J. Synthesis and characterization of a new class of anti-angiogenic agents based on ruthenium clusters. *Sci. Rep.* **2013**, *3*, 1485.
- (25) Sun, R. W.-Y.; Ng, M. F.-Y.; Wong, E. L.-M.; Zhang, J.; Chui, S. S.-Y.; Shek, L.; Lau, T.-C.; Che, C.-M. Dual anti-angiogenic and cytotoxic properties of ruthenium(III) complexes containing pyrazolato and/or pyrazole ligands. *Dalton Trans.* **2009**, 10712–10716.
- (26) Zhang, J.-J.; Sun, R. W.-Y.; Che, C.-M. A dual cytotoxic and anti-angiogenic water-soluble gold(III) complex induces endoplasmic reticulum damage in HeLa cells. *Chem. Commun.* **2012**, *48*, 3388–3390.
- (27) Kastl, A.; Wilbuer, A.; Merkel, A. L.; Feng, L.; Di Fazio, P.; Ocker, M.; Meggers, E. Dual anticancer activity in a single compound: visible-light-induced apoptosis by an antiangiogenic iridium complex. *Chem. Commun.* **2012**, *48*, 1863–1865.
- (28) Samper, K.; Rodríguez, V.; Ortega-Carrasco, E.; Atrian, S.; Maréchal, J.; Cutillas, N.; Zamora, A.; de Haro, C.; Capdevila, M.; Ruiz, J.; Palacios, Ó. Understanding the interaction of an antitumoral platinum(II) 7-azaindolate complex with proteins and DNA. *Biometals* **2014**, *27*, 1159–1177.
- (29) Ruiz, J.; Rodríguez, V.; de Haro, C.; Espinosa, A.; Pérez, J.; Janiak, C. New 7-azaindole palladium and platinum complexes: crystal structures and theoretical calculations. In vitro anticancer activity of the platinum compounds. *Dalton Trans.* **2010**, *39*, 3290–3301.
- (30) Cutillas, N.; Martínez, A.; Yello, G. S.; Rodríguez, V.; Zamora, A.; Pedreño, M.; Donaire, A.; Janiak, C.; Ruiz, J. Anticancer C,N-cycloplatinated(II) complexes containing fluorinated phosphine ligands: synthesis, structural characterization, and biological activity. *Inorg. Chem.* **2013**, *52*, 13529–13535.
- (31) Ruiz, J.; Rodríguez, V.; Cutillas, N.; Espinosa, A.; Hannon, M. J. Novel C,N-chelate platinum(II) antitumor complexes bearing a lipophilic ethisterone pendant. *J. Inorg. Biochem.* **2011**, *105*, 525–531.
- (32) Cai, G.; Fu, Y.; Li, Y.; Wan, X.; Shi, Z. Indirect ortho functionalization of substituted toluenes through ortho olefination of N,N-dimethylbenzylamines tuned by the acidity of reaction conditions. *J. Am. Chem. Soc.* **2007**, *129*, 7666–7673.
- (33) Bhattacharyya, S. Reductive alkylation of dimethylamine using titanium(IV) isopropoxide and sodium borohydride: an efficient, safe, and convenient method for the synthesis of N,N-dimethylated tertiary amines. *J. Org. Chem.* **1995**, *60*, 4928–4929.
- (34) De Vries, T. S.; Prokofjevs, A.; Harvey, J. N.; Vedejs, E. Superelectrophilic intermediates in nitrogen-directed aromatic borylation. *J. Am. Chem. Soc.* **2009**, *131*, 14679–14687.
- (35) Albrecht, M. Cyclometalation using d-block transition metals: fundamental aspects and recent trends. *Chem. Rev.* **2010**, *110*, 576–623.
- (36) Ruiz, J.; Lorenzo, J.; Vicente, C.; López, G.; López-de-Luzuriaga, J. M.; Monge, M.; Avilés, F. X.; Bautista, D.; Moreno, V.; Laguna, A. New palladium(II) and platinum(II) complexes with 9-aminoacridine: structures, luminescence, theoretical calculations, and antitumor activity. *Inorg. Chem.* **2008**, *47*, 6990–7001.
- (37) Talancón, D.; López, C.; Font-Bardía, M.; Calvet, T.; Quirante, J.; Calvis, C.; Messeguer, R.; Cortés, R.; Cascante, M.; Baldomà, L.; Badia, J. Diastereomerically pure platinum(II) complexes as antitumoral agents.: The influence of the mode of binding $\{\text{N},(\text{N},\text{O})-\text{ or }(\text{C},\text{N})\}-$ of $(1S,2R)[(\eta^5\text{-C}_5\text{H}_5)\text{Fe}\{(\eta^5\text{-C}_5\text{H}_4)\text{CHNC-(Me)CH(OH)C}_6\text{H}_5\}]$ and the arrangement of the auxiliary ligands. *J. Inorg. Biochem.* **2013**, *118*, 1–12.
- (38) Ruiz, J.; Villa, M. D.; Rodríguez, V.; Cutillas, N.; Vicente, C.; López, G.; Bautista, D. A novel metal-binding mode of thymine nucleobases: N(3) and O(4) chelation. *Inorg. Chem.* **2007**, *46*, 5448–5449.
- (39) Althoff, G.; Ruiz, J.; Rodríguez, V.; Lopez, G.; Pérez, J.; Janiak, C. Can a single C-H···F-C hydrogen bond make a difference? Assessing the HF bond strength from 2-D ^1H - ^{19}F CP/MAS NMR. *CrystEngComm* **2006**, *8*, 662–665.
- (40) Habib, H. A.; Hoffmann, A.; Höppe, H. A.; Steinfeld, G.; Janiak, C. Crystal structure solid-state cross polarization magic angle spinning ^{13}C NMR correlation in luminescent d^{10} metal-organic frameworks constructed with the 1,2-bis(1,2,4-triazol-4-yl)ethane ligand. *Inorg. Chem.* **2009**, *48*, 2166–2180.
- (41) Wisser, B.; Janiak, C. Chiral metal complexes with the biologically active (+)-pilocarpine ligand: $[\text{MCl}_2(\kappa\text{N}-(+)\text{-pilocarpine})_2]$ ($\text{M} = \text{Co, Cu}$). *Z. Anorg. Allg. Chem.* **2007**, *633*, 1796–1800.
- (42) Desiraju, G. R. S. T. The weak hydrogen bond. In *IUCr Monograph on Crystallography*; Oxford Science: Oxford, 1999; Vol. 9.
- (43) Nishio, M. The CH/ π hydrogen bond in chemistry. Conformation, supramolecules, optical resolution and interactions involving carbohydrates. *Phys. Chem. Chem. Phys.* **2011**, *13*, 13873–13900.
- (44) Nishio, M.; Umezawa, Y.; Honda, K.; Tsuboyama, S.; Suezawa, H. CH/ π hydrogen bonds in organic and organometallic chemistry. *CrystEngComm* **2009**, *11*, 1757–1788.
- (45) Nishio, M. CH/ π hydrogen bonds in crystals. *CrystEngComm* **2004**, *6*, 130–158.
- (46) Janiak, C.; Temizdemir, S.; Dechert, S.; Deck, W.; Girmsdies, F.; Heinze, J.; Kolm, M. J.; Scharmann, T. G.; Zipf, O. M. Binary [Hydrotris(indazol-1-yl)borato]metal complexes, $\text{M}(\text{Tp}_4\text{Bo})_2[1]$ with $\text{M} = \text{Fe, Co, Ni, Cu, and Zn}$: electronic properties and solvent-dependent framework structures through C-H··· π interactions. *Eur. J. Inorg. Chem.* **2000**, *2000*, 1229–1241.
- (47) Umezawa, Y.; Tsuboyama, S.; Honda, K.; Uzawa, J.; Nishio, M. CH/ π interaction in the crystal structure of organic compounds. A database study. *Bull. Chem. Soc. Jpn.* **1998**, *71*, 1207–1213.
- (48) Nishio, M. H.; Hirota, M.; Umezawa, Y. *The CH/ π interaction (evidence, nature and consequences)*; Wiley-VCH: New York, 1998.
- (49) Yang, X.-J.; Drepper, F.; Wu, B.; Sun, W.-H.; Haehnel, W.; Janiak, C. From model compounds to protein binding: syntheses, characterizations and fluorescence studies of $[\text{Ru}^{II}(\text{bipy})(\text{terpy})\text{L}]^{2+}$ complexes (bipy = 2,2'-bipyridine; terpy = 2,2':6',2"-terpyridine; L = imidazole, pyrazole and derivatives, cytochrome c). *Dalton Trans.* **2005**, 256–267.
- (50) Janiak, C. A critical account on π - π stacking in metal complexes with aromatic nitrogen-containing ligands. *J. Chem. Soc., Dalton Trans.* **2000**, 3885–3896.

- (51) Wang, D.; Lippard, S. J. Cellular processing of platinum anticancer drugs. *Nat. Rev. Drug Discovery* **2005**, *4*, 307–320.
- (52) Kelland, L. R.; Barnard, C. F.; Mellish, K. J.; Jones, M.; Goddard, P. M.; Valenti, M.; Bryant, A.; Murrer, B. A.; Harrap, K. R. A novel trans-platinum coordination complex possessing in vitro and in vivo antitumor activity. *Cancer Res.* **1994**, *54*, 5618–5622.
- (53) Elmore, S. Apoptosis: a review of programmed cell death. *Toxicol. Pathol.* **2007**, *35*, 495–516.
- (54) Guan, Y.; Shi, R.; Li, X.; Zhao, M.; Li, Y. Multiple binding modes for dicationic hoechst 33258 to DNA. *J. Phys. Chem. B* **2007**, *111*, 7336–7344.
- (55) Khoo, C. P.; Micklem, K.; Watt, S. M. A comparison of methods for quantifying angiogenesis in the Matrigel assay in vitro. *Tissue Eng. Part C, Methods* **2011**, *17*, 895–906.
- (56) Aranda, E.; Owen, G. I. A semi-quantitative assay to screen for angiogenic compounds and compounds with angiogenic potential using the EA.hy926 endothelial cell line. *Biol. Res.* **2009**, *42*, 377–389.
- (57) Hu, J.; Verkman, A. S. Increased migration and metastatic potential of tumor cells expressing aquaporin water channels. *FASEB J.* **2006**, *20*, 1892–1894.
- (58) Price, J. H.; Williamson, A. N.; Schramm, R. F.; Wayland, B. B. Palladium(II) and platinum(II) alkyl sulfoxide complexes. Examples of sulfur-bonded, mixed sulfur- and oxygen-bonded, and totally oxygen-bonded complexes. *Inorg. Chem.* **1972**, *11*, 1280–1284.
- (59) Ryabov, A. D.; Kuz'mina, L. G.; Dvortsova, N. V.; Stufkens, D. J.; van Eldik, R. Bridging of platinacycles by cis-azobenzenes: synthesis and photochemical study. Structure of the twisted inorganic Z-1,1,2,2-tetrasubstituted diazaethene [(Z)-(1,2-diphenyldiazaethene)bis-[chloro(((dimethylamino)methyl)phenyl-C_N)platinum(II)]]. *Inorg. Chem.* **1993**, *32*, 3166–3174.
- (60) Meijer, M. D.; Kleij, A. W.; Williams, B. S.; Ellis, D.; Lutz, M.; Spek, A. L.; van Klink, G. P. M.; van Koten, G. Construction of supported organometallics using cycloplatinated arylamine ligands. *Organometallics* **2002**, *21*, 264–271.
- (61) Sheldrick, G. M. A short history of SHELX. *Acta Crystallogr. A* **2008**, *64*, 112–122.
- (62) Sheldrick, G. M. *Program SADABS*; University of Göttingen, Göttingen, Germany, 1996.
- (63) DIAMOND 3.2 for Windows; Crystal Impact Gbr, B: Germany, <http://www.crystalimpact.com/diamond>.
- (64) Chen, T. R. Microscopic demonstration of mycoplasma contamination in cell cultures and cell culture media. *TCA Manual* **1975**, *1*, 229–232.